OFFICE OF NAVAL RESEARCH

GRANT or CONTRACT: N00014-91-J-1919

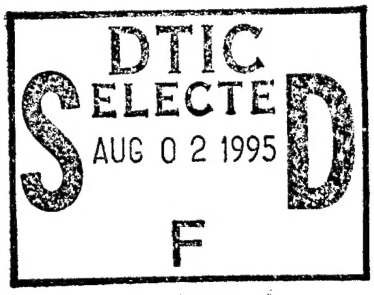

R&T Code 4133036
Robert Nowak

Technical Report No. 17

Ultrahigh Vacuum Surface Analytical Methods in Electrochemical Studies of Single-Crystal Surfaces

Manuel P. Soriaga, David A. Harrington,
John L. Stickney and Andrzej Wiechowski

In Press

for

Modern Aspects of Electrochemistry

Department of Chemistry
University of Georgia
Athens, GA 30602-2556

7/20/95

REPORT DOCUMENTATION PAGE

Form Approved
OMB No. 0704-0188

1. AGENCY USE ONLY (Leave blank)	2. REPORT DATE	3. REPORT TYPE AND DATES COVERED
	July 21, 1995	Technical - 6/1/94 - 5/31/95

4. TITLE AND SUBTITLE

Ultrahigh Vacuum Surface Analytical Methods in Electrochemical Studies of Single-Crystal Surfaces

5. FUNDING NUMBERS

G-N00014-91-J-1919
Dr. Robert J. Nowak
R&T Code: 4133036

6. AUTHOR(S)

Manuel P. Soriaga, David A. Harrington, John L. Stickney and Andrzej Wieckowski

7. PERFORMING ORGANIZATION NAME(S) AND ADDRESS(ES)

John L. Stickney
Department of Chemistry
University of Georgia
Athens, GA 30602-2556

8. PERFORMING ORGANIZATION REPORT NUMBER

Technical Report # 17

9. SPONSORING/MONITORING AGENCY NAME(S) AND ADDRESS(ES)

Office of Naval Research
Chemistry Division
800 North Qunicy Street
Arlington, VA 22217-5660

10. SPONSORING/MONITORING AGENCY REPORT NUMBER

11. SUPPLEMENTARY NOTES

For publication in "Modern Aspects of Electrochemistry"
Editors J. O'M. Bockris, B.E. Conway and R.E. White

12a. DISTRIBUTION/AVAILABILITY STATEMENT

Approved for public release and sale;
its distribution is unlimited

12b. DISTRIBUTION CODE

13. ABSTRACT *(Maximum 200 words)*

A complete understanding of a given electrochemical reaction needs to take into account all the physical and chemical interactions that arise between an electified surface and the constituents of the electrolytic environment. Such interactions will depend upon the parameters which control the properties of the electrode-solution interface; these include solvent, electrolyte, electrode potential, reactant concentration, crystallographic orientation, and surface electronic structure. The traditional approach to the study of the electrode-solution interface is based upon a thermodynamic analysis of the interfacial response to perturbations in terms of current-charge-potential measurements. Analysis of results from such measurements have relied on phenomenological methods which incorporate, to varying levels of approximation, the macroscopic interfacial parameters, devoid of atomic-level specificity.

The need for an atomic-level perspective of electrochemical processes is now well established. While it is true that a great deal is now known about heterogeneous processes at gas-solid interfaces, it should be noted that barely two decades ago, these fields were beset by problems remarkably similar to those today.

14. SUBJECT TERMS	15. NUMBER OF PAGES
UHV Surface Analysis, Single Crystal Electrochemistry	52
	16. PRICE CODE

17. SECURITY CLASSIFICATION OF REPORT	18. SECURITY CLASSIFICATION OF THIS PAGE	19. SECURITY CLASSIFICATION OF ABSTRACT	20. LIMITATION OF ABSTRACT
Unclassified	Unclassified	Unclassified	UL

"Modern Aspects of Electrochemistry"
J. O'M. Bockris, B. E. Conway and R. E. White
Editors

ULTRAHIGH VACUUM SURFACE ANALYTICAL METHODS IN ELECTROCHEMICAL STUDIES OF SINGLE-CRYSTAL SURFACES

Manuel P. Soriaga
Department of Chemistry
Texas A&M University
College Station, TX 77843

David A. Harrington
Department of Chemistry
University of Victoria
Victoria, B. C. V8W 2Y2

John L. Stickney
Department of Chemistry
University of Georgia
Athens, GA 30602

Andrzej Wieckowski
Department of Chemistry
University of Illinois
Urbana, IL 61801

CONTENTS

I. INTRODUCTION

A complete understanding of a given electrochemical reaction needs to take into account all the physical and chemical interactions that arise between an electrified surface and the constituents of the electrolytic environment. Such interactions will depend upon the parameters which control the properties of the electrode-solution interface; these include solvent, electrolyte, electrode potential, reactant concentration, crystallographic orientation, and surface electronic structure. The traditional approach to the study of the electrode-solution interface is based upon a thermodynamic analysis of the interfacial response to perturbations in terms of current-charge-potential measurements. Analysis of results from such measurements have relied on phenomenological models which incorporate, to varying levels of approximation, the macroscopic interfacial parameters, devoid of atomic-level specificity.

The need for an atomic-level perspective of electrochemical processes is now well established [1-7]. While it is true that a great deal is now known about heterogeneous processes at gas-solid interfaces, it should be noted that barely two decades ago, these fields were beset by problems remarkably similar to those presently facing interfacial electroanalytical chemistry. For example, research in vacuum-solid surface science traditionally employed work function measurements and thermal desorption spectroscopy which, respectively analogous to electrochemical capacitance measurements and cyclic voltammetry, do not yield atomic-level information. Thus, basic questions, such as the chemical nature of the adsorbed species or the atomic geometry of the adsorbate-substrate interface, could not be answered by data provided by these methods. It was not until the development of powerful surface-specific experimental [8-13] and theoretical [14-21] tools that tremendous gains in the study of the gas-solid interface were achieved. This overwhelming success motivated the adaptation of such surface-sensitive

probes to the study of the electrode-solution interface [22-28].

Most of these methods are based upon the mass-analysis of molecules or the energy-analysis of electrons, ions, or atoms scattered/emitted from solid surfaces. The shallow escape depths of these particles make their use most suitable for interfacial studies since the information they bear is characteristic of the near-surface layers; on the other hand, their short mean-free paths necessitate a high vacuum environment. The application of such techniques to electrochemical systems requires that the interfacial characterization be performed outside the electrochemical cell; the results obtained have been so dramatic in atomic-level detail. A comprehensive review of the UHV-EC approach has recently been published [28].

2. EXPERIMENTAL PROTOCOLS

A. Electrode-surface preparation

While many vacuum-based surface analytical methods do not require the use of single-crystal surfaces, for fundamental work such as those that perform surface crystallographic measurements, the use of uniform (monocrystalline) surfaces becomes a desirable component. In such atomic-level investigations, the preparation *and* verification of clean and well-ordered electrode surfaces constitute critical initial steps. The low-index surface crystallographic faces, such as the (111), (110), and (100) planes of face-centered cubic crystals, have been widely used because of their low surface free energies, high symmetries, and relative stabilities. In addition, it can be argued that the resultant macroscopic behavior of smooth polycrystalline electrodes can be constructed in terms of the individual properties of these three surface planes [8,29-35].

Three procedures have been used to prepare oriented monocrystalline electrode surfaces. In one method, single-crystal rods or boules, usually grown by zone-refining, are oriented by the Laué back-reflection technique [36] and then cut

along the desired crystal face. A second procedure is based on the fact that spherical single crystals are obtained when a polycrystalline Pt wire is melted in a gas-oxygen flame [33,37]. Metallographic polishing is subsequently performed on the oriented crystals obtain a uniformly smooth surface. The oriented and polished monocrystalline microelectrodes are re-annealed at near-melting temperatures to repair the damaged selvedge. A third scheme, limited to (111) faces, involves epitaxial growth by vapor deposition onto a hot (400°C) mica substrate. Atomically smooth and well-ordered Au(111) and Ag(111) single-crystal thin-film electrodes have been prepared in this manner [38-40].

If the entire single-crystal electrode is to be immersed in solution for electrochemical experiments, it is necessary to prepare a *parallelipiped* crystal in which all six faces are oriented identically. It is possible to fabricate an electrochemical cell such that only one oriented face will be in contact with electrolyte. This configuration would permit the use of a disc electrode (in which only one face is oriented and polished) or a multi-faceted crystal (in which each face represents a distinct crystallographic orientation).

The oriented single crystal electrodes require further pretreatment before reliably clean and ordered surfaces are obtained. There are two general schemes: one employs high temperatures (thermal annealing) [8-11,22-28], the other applies electrode potentials (electrochemical annealing) [41-46]. Thermal annealing in UHV serves a dual purpose: to segregate bulk contaminants onto the surface (where they can be oxidatively desorbed or sputtered away), and to obtain atomic smoothness. Surface analysis is subsequently performed to ascertain interfacial structure and composition; surfaces subjected to such analysis are considered truly *well-defined*. Interfacial characterization at a qualitative level can be done by voltammetric methods if reference data for well-characterized electrode surfaces are available [32,47-49]. Electrochemical annealing is based on the possibility that, at appropriate potentials, disordered interfacial atoms can either be activated to diffuse to stable

(ordered) sites or be dissolved to expose ordered layers (electropolishing). Electrode potential-induced surface reconstruction [41] may occur unassisted or assisted by electrolyte. The electrochemical ordering of Au (111) electrodes by sequential voltammetric scans between the oxygen and hydrogen evolution regions [50,51] is an example of the former case. The ordering of Pd(111) surfaces by potentiodynamic scans in the region where the iodide electrolyte undergoes reversible oxidative adsorption/reductive desorption is electrolyte-assisted since it is the strong chemisorption of iodine which provides the driving force in the disorder-to-order surface reconstruction [42-44]. Subsequent cathodic desorption of the absorbed iodine yields a clean and well-ordered Pd(111) surface [42]. In the electrochemical annealing of Au(111) and Pd(111), no electrode dissolution occurs, as opposed to microscopic electropolishing exhibited by reactive materials such as Ag (in $NaCN/H_2O_2$ solution [45]) or Cu in acidic media [46] in which the damaged surface layers are anodically etched away.

The preservation of the single crystallinity of electrode surfaces is also an important consideration. In most cases, conditions are known at which the surface single crystallinity can be maintained. For example, the single-crystal surface structure remains unchanged unless excursions are made to potentials which lead to extensive surface-oxide formation [32,42-44,52-55]. However, even if surface-oxidation potentials are averted, prolonged exposure to electrolytic solutions invariably results in the accumulation of surface impurities. In UHV-EC experiments, the regeneration of clean and ordered single-crystal surfaces from spent electrodes consists of high-temperature oxygenation or Ar^+ ion sputtering followed by a thermal treatment to restore atomic smoothness. *In situ* reordering options exist for other materials: Cu(111) by microscopic electropolishing [45,46], Au(111) and Pd(111) by electrochemical annealing [42-44,50,51].

B. Interfacial characterization techniques

The cleanliness and single crystallinity of electrode surfaces cannot simply be assumed even if the preparative steps outlined above are followed. The verification or identification of initial, intermediate, and final interfacial structures and compositions is an essential ingredient in electrochemical surface science. Except for voltammetry of electrosorption/desorption reactions and coulometry of adsorbate redox reactions, interfacial characterization in UHV-EC studies rely largely on *ex situ* surface-sensitive methods that have been used with tremendous success in gas-solid interfacial studies. Although a myriad of surface-sensitive analytical techniques are currently available [8-13], those actually employed in UHV-EC experiments have been limited to low-energy electron diffraction, Auger electron spectroscopy, X-ray photoelectron spectroscopy, high-resolution electron energy loss spectroscopy, reflection high-energy electron diffraction, work-function changes, and thermal desorption mass spectrometry.

(i) Surface spectroscopy with low-energy electrons. The main difficulty in the surface characterization of single-crystal surfaces lies in the exceedingly low population of surface atoms (10^{15} atoms cm^{-2}) relative to that of bulk species (10^{23} atoms cm^{-3}). Experiments intended to examine the physical and chemical properties of surfaces must employ methods that interact only with the interfacial layers. The majority of interfacial characterization techniques [8-13] takes advantage of the unique surface sensitivity of low-energy electrons. This surface influence arises because the mean free path of an electron through a solid is dependent upon its kinetic energy. As shown in the so-called "universal curve" reproduced in Figure 1, the electron mean free path falls to a minimum (4 to 20 Å) when the kinetic energy is between 10 and 500 eV. This signifies that all experimental techniques based upon the low-energy electron incidence onto and/or emergence from surfaces will bear information on the topmost surface layers.

A solid surface subjected to a beam of electrons of incident or primary energy E_p gives rise to the appearance of backscattered (primary) and emitted (secondary)

Fig. 1. "Universal curve." Electron mean free path as a function of electron kinetic energy. Reproduced with permission [8].

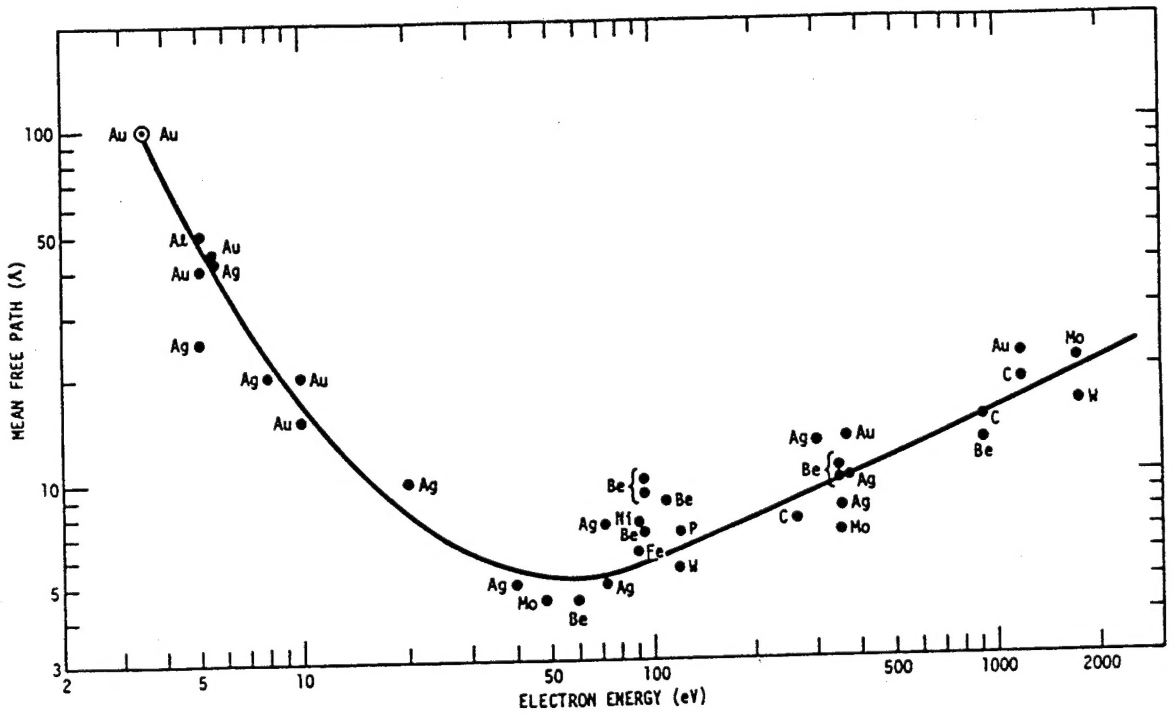

electrons; the energy distribution, a plot of the number of electrons N(E) as a function of energy E, of these electrons is shown in Figure 2. This spectrum can be divided into four regions according to the origin of the scattered electrons: (i) True *secondary* electrons, created as a result of multiple inelastic interactions between the incident and bound electrons; these electrons give rise to the prominent broad band at the lower end of the spectrum. (ii) Auger electrons emitted and primary electrons elastically scattered due to interactions with electronic states in the solid; the small peaks in the medium-energy range of the spectrum are attributed to these electrons. (iii) Primary electrons inelastically scattered upon interactions with the vibrational states of the surface; peaks resulting from these electrons reside close to the elastic peak since their energy losses are comparatively minute. (iv) Primary electrons scattered elastically; these electrons, which comprise only a few percent of the total incident electrons, give rise to the elastic peak at E_p. Regions (ii) to (iv) of the energy distribution spectrum have been exploited in modern surface analysis. The elastic peak, for example, is used in diffraction experiments; the other peaks provide information on electronic and vibrational structures.

(ii) Low-energy electron diffraction (LEED). In this method [8-13,56,57] the surface is irradiated with a monoenergetic beam of electrons and the elastically backscattered electrons are collected onto a phosphor screen. The virtue of LEED as a surface structural technique is a result of the low kinetic energies used (50 to 500 eV) since: (i) the electron mean free path is at a minimum which affords LEED its surface sensitivity; (ii) the de Broglie wavelengths, $\lambda_e \approx (150/E_e)^{1/2}$ (where E_e is in eV and λ_e is in Å) correspond to crystal lattice dimensions which render the low-energy electrons suitable for diffraction studies; and (iii) electron backscattering is strong which minimizes incident electron fluxes at, and subsequent scattering from, non-surface layers. In LEED, therefore, the presence (or absence) of diffraction patterns on the fluorescent screen is a consequence of the order (or disorder) of the atomic arrangements near the surface.

Fig. 2. Experimental number [N(E)] of scattered electrons of energy E versus electron energy. Reproduced with permission [8].

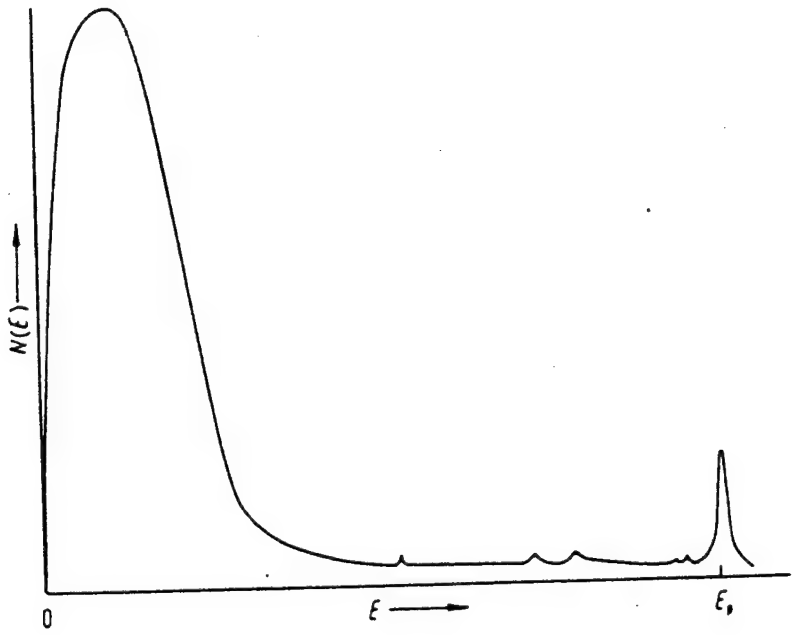

The coherence width of electron beam sources in LEED is typically 100 Å. That is, sharp diffraction features appear only if well-ordered domains are at least $(100\ Å)^2$ in size; diffraction from smaller domains leads to beam broadening. The locations of the diffracted beams define the reciprocal lattice of the real surface. The real-space surface structure itself can be reconstructed from the real-space unit cell vectors generated from the reciprocal lattice vectors according to well-known relationships [8-13,56,57].

The analysis of LEED data based solely upon the geometry of the diffraction spots provides information on the periodicity of the electron scatterers on the surface. In some favorable instances, other information such as adsorbate coverages or point group symmetries can also be inferred. However, the actual location of the atoms within the surface lattice *cannot* be determined without an analysis of the intensities of the diffracted beams. Surface crystallography by LEED can only rely upon a comparison of the measured diffraction intensities with those calculated for model structures. These LEED simulations are extremely difficult because of complications brought about by the possibility of multiple electron scattering [8-13,56,57].

For structures formed under electrochemical conditions, only single-scattering (kinematic) LEED simulations for simple atomic adsorbates have been carried out; the primary intent has simply been the qualitative verification of proposed structures. The calculations are based on the following equation [58,59]:

$$I_s = \left\{ \frac{1}{J} \sum_{i=1}^{J} a_i \exp\left[2\pi i \left(X_i X_s + Y_i Y_s + Z_i Z_s \right) / \lambda_e \right] \right\}^2 \qquad (3.3)$$

I_s is the intensity of each beam s calculated for selected kinetic energies, J the number of atoms in the unit mesh, and a_i is the scattering factor of the ith atom. X_s, Y_s, and Z_s are the Cartesian coordinates of the scattered beam where $Z_s = 1 + \cos$

θ_d, θ_d being the angle between the incident and diffracted beams.

There are two schemes for the notation of interfacial adlattice structures. The matrix notation, which is applicable to any system, is based upon the relationship between the real-space lattice vectors of the *adsorbate* mesh and the *substrate* (clean-surface) mesh [8-13,56,57]. The other method, known as the Wood notation [36], is more widely used but is applicable only if the angle between the adsorbate unit cell vectors is the same as that between substrate unit mesh vectors. The surface structure is labeled using the general form $(n\times m)R\phi°$ or $c(n\times m)R\phi°$ where c designates a centered unit cell, $R\phi°$ the angle of rotation of the adsorbate unit cell relative to the substrate unit mesh, and n and m are scale factors relating the adsorbate and substrate unit cell vectors

A schematic diagram of a typical LEED instrument is shown in Figure 3 [60]. The LEED "optics" consists of a phosphor-coated hemispherical screen at the center of which is a normal-incidence, electrostatically focused electron gun. In front are three concentric grids; the outer grid is held at ground potential, while the inner two are maintained at a voltage just below that of the electron gun in order to reject *inelastically* backscattered electrons. The elastically diffracted electrons which pass through the suppressor grids are accelerated onto the fluorescent screen by a 5 kV potential applied to the screen. For quantitative LEED intensity measurements, additional provisions are required such as the use of a movable Faraday cup, a spot photometer, or a computer-interfaced video camera.

The LEED pattern for an iodine-coated Pd(111) electrode surface is provided as an example in Figure 4; included in this figure is the suggested real-space surface structure of the Pd(111)-$(\sqrt{3}\times\sqrt{3})R30°$-I adlattice [61].

(iii) Reflection high-energy electron diffraction (RHEED). As a method for the determination of near-surface structural order, RHEED [8,11,13,62,63] represents an alternative to LEED. The principal difference between the two structural techniques is that, while low-energy electrons are utilized in LEED, RHEED

Fig. 3. Schematic diagram of a LEED apparatus. Reproduced with permission [60].

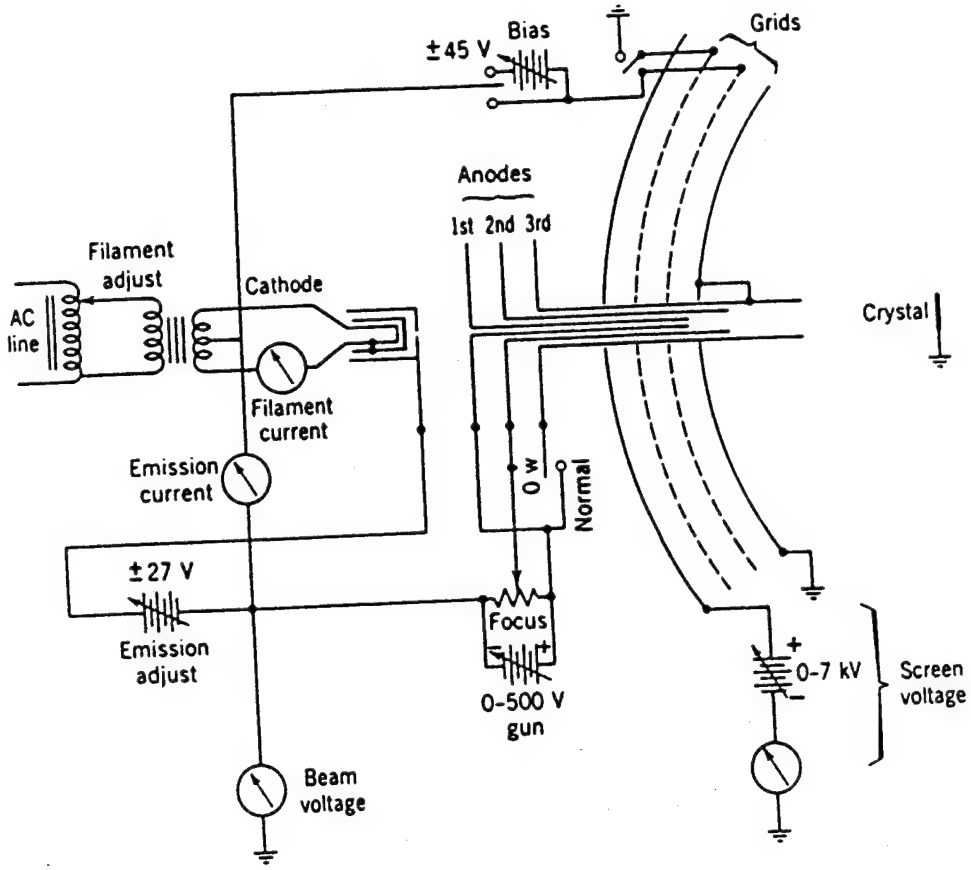

Fig. 4. LEED pattern for a Pd(111) electrode coated with iodine from dilute aqueous NaI; also shown is the postulated real-surface structure. Reproduced with permission [61].

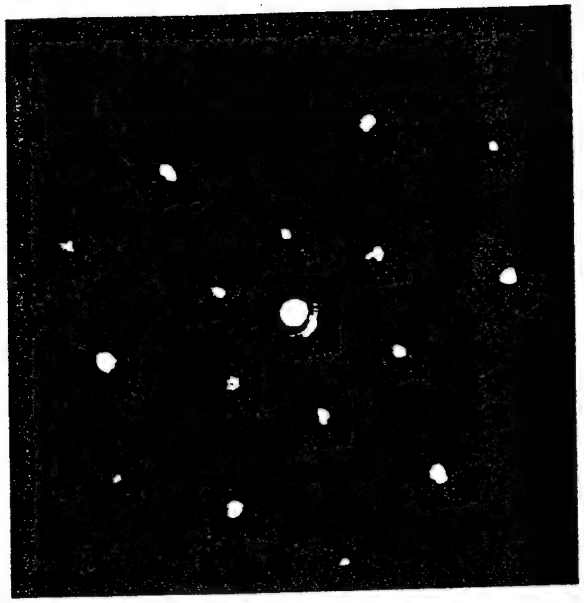

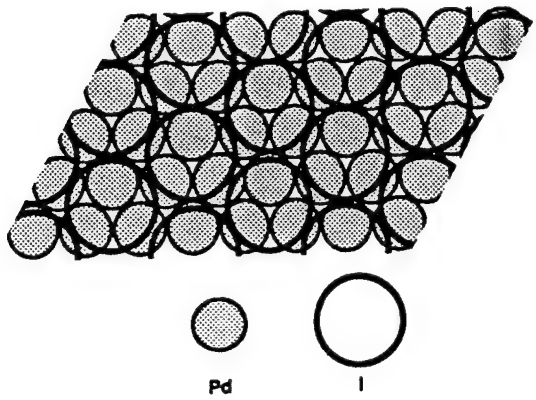

Pd(111)-($\sqrt{3}$x$\sqrt{3}$)R30°-I

employs high-energy (30 to 100 keV) electrons. At such energies, the inelastic mean-free-paths of the incident electrons are long (100 to 1000 Å) and only a very small fraction of electrons is backscattered. To afford the required surface sensitivity, RHEED experiments are performed with very small angles (< 5°) of incidence and diffraction. The requirements for energy filtering are far less stringent in RHEED than in LEED because of the large energy difference between the elastically and inelastically scattered electrons; post-acceleration is likewise unnecessary in RHEED as the primary electrons are sufficiently energetic to produce fluorescence on the phosphor screen.

Figure 5 shows LEED and RHEED patterns of gold films evaporated on glass and on mica [59]; the film deposited on glass at room temperature is rough but that on mica at elevated temperatures is smooth and well-ordered in the (111) plane. It can be seen in this figure that ordered-surface diffraction is manifested in LEED by distinct spots and in RHEED by sharp streaks.

RHEED is most useful in studies related to the structure and morphology of thin films and surface coatings. It is possible to monitor film formation continuously under deposition conditions since the front of the sample is unimpeded by either the electron source or analyzer and is thus available for placement of a film-deposition source. In view of its low-scattering-angle geometry, RHEED is quite sensitive to surface asperities. Dynamical theories for RHEED have been developed but accurate experimental data are not available for analysis [8,11,13].

(iv) Auger electron spectroscopy (AES). AES is one of the more widely used techniques for surface elemental analysis [8-13,64-78]. In the Auger process, illustrated schematically in Figure 6, a core (K) level electron is emitted when a beam of electrons, typically with energies between 2 to 10 keV, is impinged onto the sample surface. In the decay process, an electron in an upper (L_I) level falls into the vacant core level and another electron in a different upper (L_{III}) level is ejected; the second, emitted, electron is the Auger electron and this particular process is labeled

Fig. 5. LEED and RHEED patterns for Au vapor deposited onto (a) glass at room temperature, (b) glass at 400°C, and (c) mica at 360°C. Reproduced with permission [39].

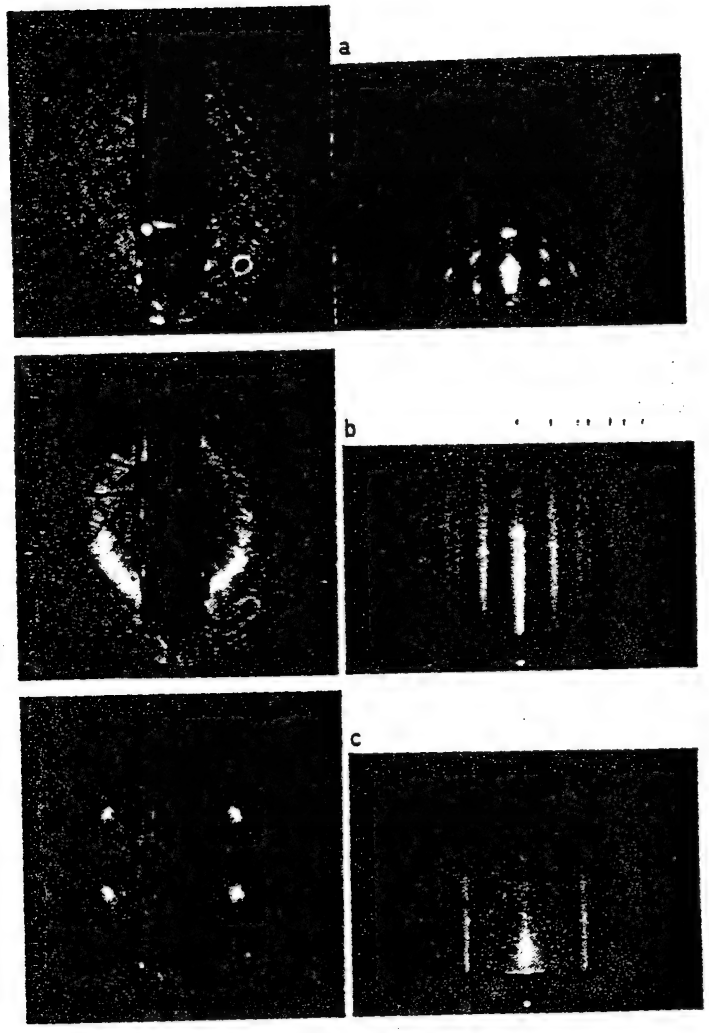

as a KL_IL_{III} in order to specify which energy levels are involved. The kinetic energy of the Auger electron is dependent upon the binding energies of the K, L_I, and L_{III} electrons but not upon the energy of the incident or primary electrons. The appropriate relationship is given by:

$$E_{KL_IL_{III}} = E_K - E_{L_I} - E_{L_{III}} - e\varphi_{sp} \qquad (3.9)$$

where e is the electronic charge and φ_{sp} the spectrometer work function. The exact application of Equation (3.9) must realize that the energy difference is actually between singly ionized (one-hole) and doubly ionized (two-hole) binding energy states. Nevertheless, $E_{KL_IL_{III}}$, as obtained from empirical spectra is characteristic of a given atom which affords AES its element-specificity. Since the overall Auger process involves three electrons, AES is clearly not applicable for the analysis of H and He. It should also be noted that, although the incident electrons are of high energies, AES is still a surface-sensitive method because the emitted Auger electrons are generally of much lower energies and correspond to the minimum in the universal curve (Figure 1).

An inherent difficulty in AES arises from the fact that the Auger emission peaks are actually of very low intensities superimposed on a large secondary emission background (Figure 2). The usual approach to circumvent this problem is the combination of electron-energy analysis with suitable modulation techniques; in this manner, spectra exclusive of the original background can be obtained. The two more common energy analyzers used in AES are the retarding field (RFA) and cylindrical mirror analyzers (CMA). In a multi-technique instrumentation that includes LEED, an RFA is most affordable since it makes use of the LEED optics (Figure 3). Energy analysis with an RFA involves the application of a voltage ramp to the suppressor grids such that only electrons of energies higher than the applied potential are transmitted through and accelerated onto the screen which is kept at a

Fig. 6. Schematic diagram of the Auger emission process. The core (K) level electron is that which is ejected in X-ray photoelectron spectroscopy, while the Auger electron is the ejected electron designated as KL_IL_{III}. Reproduced with permission [8].

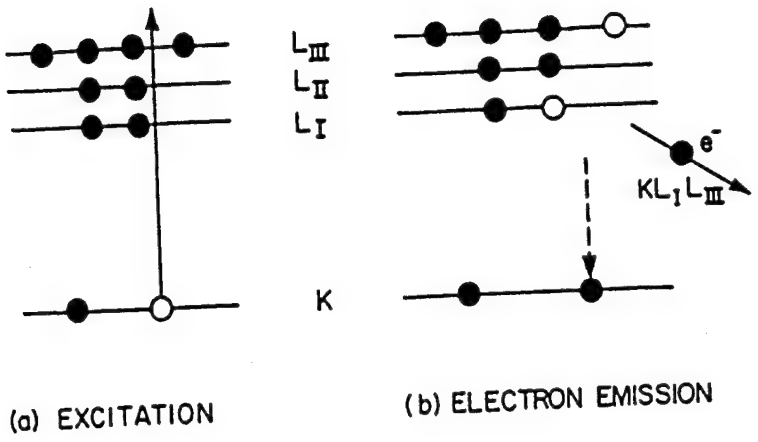

high positive (1 kV) voltage. In modulated RFA, the retarding voltage is modulated, typically at 1 kHz, with a 5 V (peak-to-peak) signal. The modulated component of the signal arriving at the screen is then passed to a lock-in amplifier tuned to a frequency twice that of the suppressor grid modulation (second-harmonic). The end result is a derivative signal, dN(E)/dE, devoid of the original large background.

Because of important advantages over an RFA, such as higher sensitivity and resolution, Auger electron spectroscopy with a CMA is now more widely used. A schematic diagram of a CMA is given in Figure 7. Energy analysis with a CMA is achieved by a negative ramp voltage applied to the outer cylinder while the inner cylinder is held at ground. Only electrons of the appropriate energy can pass unhindered through the CMA and into the detector which is usually a channel electron multiplier. As with modulated RFA, the pass energy of the CMA is modulated and then synchronously demodulated with a lock-in amplifier. The resultant spectrum is also a derivative spectrum. It should be noted that modern instruments now employ software-based modulation and filtering. The resolution of a CMA is dependent upon its entrance and exit slits; improved resolution can be achieved by a double-pass CMA. Improved resolution is also afforded by the use of a cylindrical hemisphere analyzer (CHA) which, as described below, is inherently a double-focusing analyzer.

A surface of a given composition possesses a signature Auger dN(E)/dE spectrum; this renders AES a powerful technique for qualitative surface elemental analysis. An example is given in Figure 8 for a Au(111) surface electrodeposited with Te prior to formation of CdTe [79]. For quantitative and/or molecular compositional analysis [64-67], the derivative spectrum is difficult to process. An approach to the collection of standard (non-derivative) Auger spectra involves pulse counting electronics or direct current measurements; spectra generated in this manner have been deconvoluted by a fast Fourier transform algorithm [68,69] to obtain information on chemical shifts and lineshapes. Changes in Auger lineshapes

Fig. 7. Schematic cross section of a cylindrical mirror analyzer. U_a is the potential applied between the two coaxial cylindrical electrodes, $\Delta\gamma$ is the angular spread of the electrons at the entrance slit, and $i(U_a)$ is the current at the exit aperture Reproduced with permission [10].

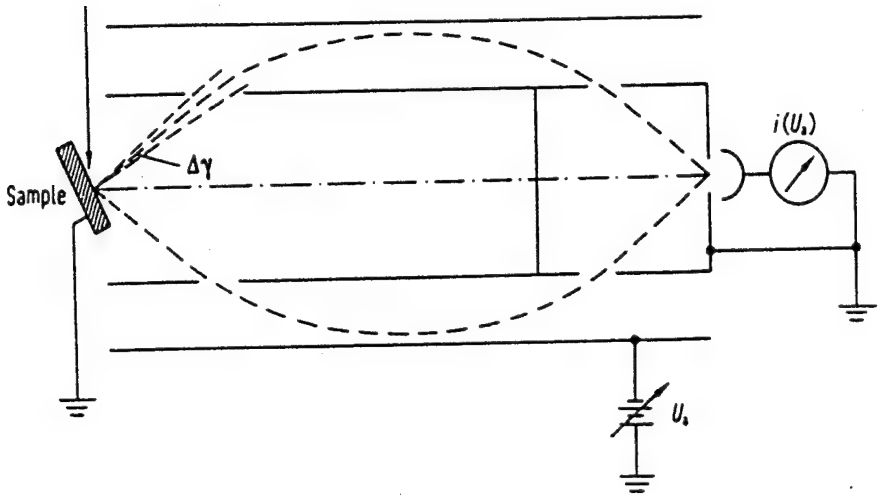

Fig. 8. AES spectra for a Au(111) substrate before (a) and after (b-g) deposition of various amounts of Te. Reproduced with permission [79].

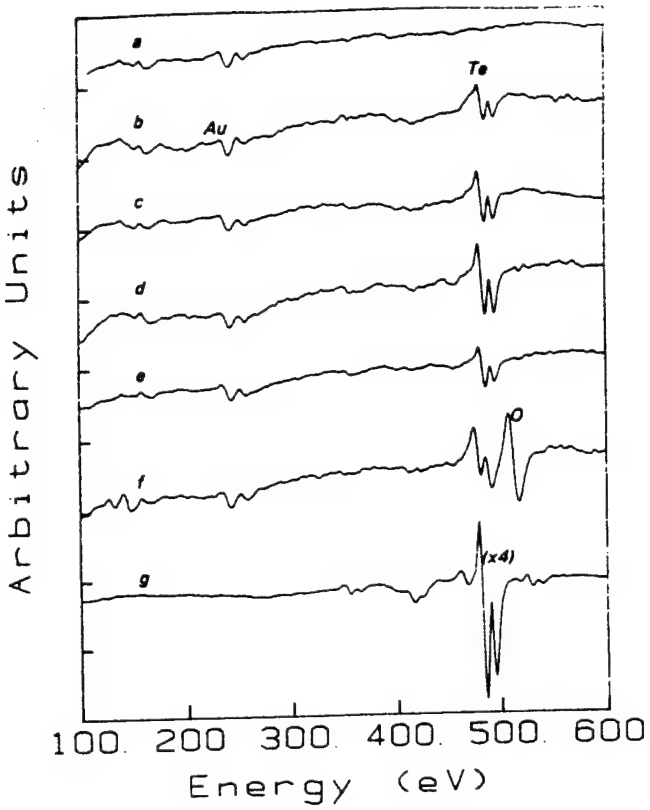

reflect modifications in the valence band density of states.

The use of derivative Auger spectra for the determination of adsorbate surface coverages has been the subject of numerous studies [89-92]. One method, specifically used in surface electrochemical studies, makes use of the following equation [74-76]:

$$\Gamma_a = \frac{I_a}{I_p \phi_c G_a} \tag{3.10}$$

where Γ_a is the absolute packing density of the adsorbate (mole cm^{-2}), I_a the Auger current for the adsorbate, I_p the primary beam current, ϕ_c the measured collection efficiency of the Auger spectrometer, and G_a is the *calculated* Auger electron yield factor [80]. I_a is obtained by double integration of the adsorbate *second-harmonic* amplitude A_2 corrected for the clean-surface signal A_{2c} [72,73]:

$$I_a = \frac{4}{k^2} \int_0^{E_p} \int_0^{E} (A_2 - \phi_b A_{2c})\, dE'\, dE \tag{3.11}$$

where ϕ_b is the observed attenuation of the substrate signal by the adsorbed species, and k is the modulation amplitude. For simple adsorbates for which well-characterized surface layers are available for calibration purposes, Equation (3.10) can be expressed in purely empirical terms [75,76]:

$$\Gamma_a = \left(\frac{I_a}{I^o_M}\right)\frac{1}{B_a} \tag{3.12}$$

where I^o_M is the Auger signal for the clean substrate, and B_a is a calibration factor.

(v) X-ray photoelectron spectroscopy (XPS). This technique [8-13,81,82],

originally referred to as electron spectroscopy for chemical analysis (ESCA) [83] is the other widely used method for surface compositional analysis. In XPS, which is based upon the photoelectric effect, the solid surface is irradiated with X-rays which results in the ejection of a core-level electron. The kinetic energy E_{Kin} of the emitted photoelectron is given by:

$$E_{Kin} = h\nu - E_B - e\varphi_{sp} \tag{3.13}$$

where $h\nu$ is the energy of the incident X-ray photon and E_B, within the framework of Koopman's theorem, is the binding energy of the core-level electron. If E_B is to be referred to the vacuum level, the spectrometer work function φ_{sp} must be known. For studies with metals, it is more convenient to reference E_B with respect to the Fermi level; the latter is readily determined since it is marked by the onset of electron emission at the highest kinetic energy.

The XPS source consists of an anode material which, upon bombardment by high-energy electrons, emits X-rays. The emitted radiation can be rendered monochromatic by Bragg diffraction or by the use of the characteristic emission lines of the anode; for Mg and Al, commonly used as anodes, these lines are 1253.6 eV (Mg-Kα) and 1486.6 eV (Al-Kα), respectively. With the availability of synchrotron radiation, continuous, high-flux X-rays can be obtained. It is important to note that, for $E_B < 700$ eV and using either a Mg or Al source, the E_{Kin} of the ejected photoelectron will *not* fall within the minimum of the universal curve. In such case, the surface sensitivity of XPS becomes minimal. This can be remedied either by the use of near-grazing incidence or by the detection of electrons emitted at small angles with respect to the surface plane.

To afford the high resolution required for meaningful XPS studies, energy analysis is usually based upon a CHA, a diagram of which is presented in Figure 9. A potential difference U_k is applied across the inner and outer hemispheres of radii

Fig. 9. Schematic cross section of the concentric hemisphere analyzer. Reproduced with permission [10].

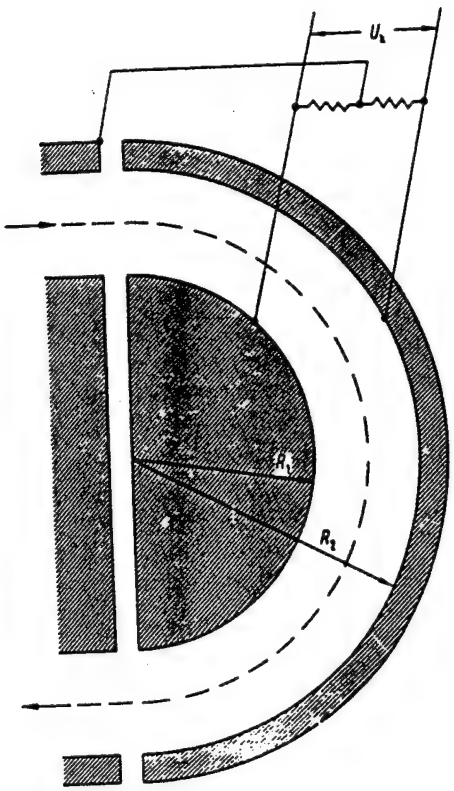

R_1 and R_2, respectively. Electrons of energy eV_e are focused at the exit slit only if the following equation is satisfied:

$$U_k = V_e\left(\frac{R_2}{R_1} - \frac{R_1}{R_2}\right) \tag{3.14}$$

The CHA is double focusing since it focuses in two planes. The resolution of a CHA can be improved significantly by electron pre-retardation with an RFA or a retarding lens system. XPS has also been performed with a double-pass CMA. Detection is typically with a channel electron multiplier. Due to inherently weak intensities, signal averaging and other data processing routines are always employed.

Qualitative elemental analysis of sample surfaces relies upon the comparison of measured E_B values with those for reference materials. Quantitative analysis is based on the fact that the ionization cross-section of a core electron is essentially independent of the valence state of the element. Hence, the intensity will always be proportional to the number of atoms within the detected volume. For quantitative purposes, the area under the background-corrected peak is taken as the intensity. The intensity is a complicated function of several parameters some of which can be eliminated by the use of a reference state analyzed under identical conditions as the sample; however, such favorable cases are infrequent. If the spectrometer has a small aperture and the surface is uniformly irradiated, the equation for the intensity can be simplified to:

$$I_A = \sigma_A D L_A J_0 N_A \lambda_M G_1 \cos\theta_1 \tag{3.15}$$

where I_A is the integrated peak intensity for an element A, σ_A the photoionization cross section, D the spectrometer detection efficiency, L_A the angular asymmetry of the emitted intensity with respect to the angle between the incidence and detection

directions, J_o the flux of primary photons, N_A density of atoms A, λ_M the escape depth of the photoelectron, G_1 the spectrometer transmission, and θ_1 is the angle between the surface normal and the detection direction. The application of Equation (3.15) for various adsorbate-substrate configurations has been the subject of extensive discussion [8-13,84].

As a surface elemental analysis tool, XPS is complementary to AES. Since the ionization cross-section for an Auger process decreases with E_B, which in turn increases with atomic number Z, AES is most sensitive to $Z < 45$ elements; for heavier elements, XPS provides higher sensitivity. The one distinct advantage that XPS offers is in the determination of oxidation states of the elements under examination. This is easily done in XPS because the binding energies of the core-level electrons are influenced by changes in chemical environment. In principle, identical information can be obtained from Auger peak energy shifts and lineshapes; in practice, however, the extraction of such information from raw derivative or non-derivative AES spectra is not a trivial task [65-69].

Example XPS spectra, those of a smooth polycrystalline Ir foil electrode containing surface before and after pretreatment with iodine, are shown in Figure 10; the peaks at 62.1 and 65.2 eV represent surface iridium oxide [85].

(vi) High-resolution electron energy loss spectroscopy (HREELS). Almost all of the incident electrons impinged at a solid surface undergo inelastic events that cause them to be backscattered at energies lower than the primary energy E_p. If E_l is the energy lost to the surface, peaks would appear in the energy distribution spectrum (Figure 2) at energies $\Delta E = E_p - E_l$. Such peaks, commonly referred to as electron energy loss peaks, are of several types according to the origin of the energy loss; these types include core-level ionization, valence-level excitations, plasmon losses, and vibrational excitations. For the latter, the energy losses are small since $E_{vib} < 4000\ cm^{-1} \approx 0.5$ eV. Hence, the loss peaks due to vibrational interactions at $\Delta E = E_{vib}$ lie close to the elastic peak and can be observed only if electron energy

Fig. 10. X-ray photoelectron spectra for a smooth polycrystalline Ir foil electrode before and after pretreatment with iodine. Reproduced with permission [85].

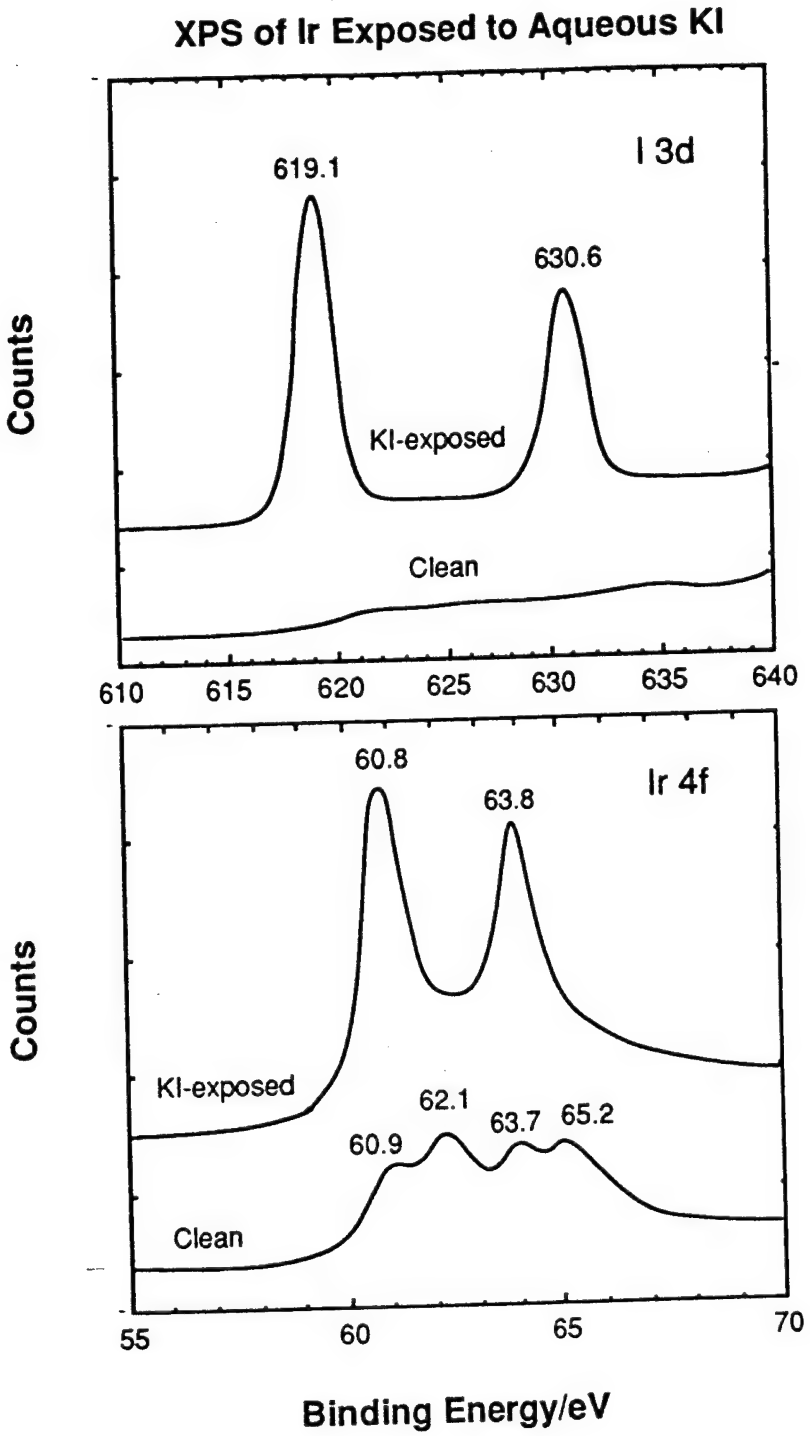

loss measurements are done at high resolution.

At solid surfaces, there are two mechanisms that give rise to vibrational HREELS spectra [8-13,86,87]: dipole scattering and impact scattering. In dipole scattering, the incident electron interacts with the oscillating electric dipole moment induced by the vibration of species at the surface. Such interactions occur at long range and can be described either classically or quantum mechanically. Two important selection rules apply for surface dipole scattering: (i) Only vibrations whose dynamic dipole moments perpendicular to the surface are non-zero contribute to HREELS spectra. This selection rule is the same as that for surface infrared reflection-absorption spectroscopy (IRAS) [88-102]. (ii) The intensity distribution with respect to scattering angle is sharply peaked in the specular direction; that is, loss peaks due to dipole scattering disappear when the backscattered electrons are collected at an angle different from that of the specularly reflected beam.

The mechanism for impact scattering at solids, which can only be treated quantum mechanically, involves exceedingly short-range interactions between the incident electron and the oscillator at the surface. The surface dipole selection rules do not apply to impact scattering. Theoretical considerations have predicted, and experimental studies have confirmed, the following properties of this type of scattering mechanism [86,87]: (i) Impact scattering vanishes in the specular direction; that is, loss peaks due to impact scattering can be observed only if the scattered electrons are detected at angles removed from the specular direction. The dependence of dipole and impact scattering on off-specular scattering angle (φ) is demonstrated by the data in Figure 11 [103]. (ii) Impact scattering is more likely to prevail at higher energies. (iii) Strong dipole scatters are weak impact scatterers; conversely, weak dipole scatterers are strong impact scatterers.

It is clear that the combination of specular and off-specular HREELS could provide a means for the complete identification of the normal modes of an adsorbed molecular species; point and space group theoretical considerations would of course

Fig. 11. The angular profile of electrons scattered inelastically from an ordered monolayer of H on W(100). The 80-meV mode is parallel whereas the 130-meV vibration is perpendicular to the surface. The 260-meV mode is the first overtone. Reproduced with permission [86].

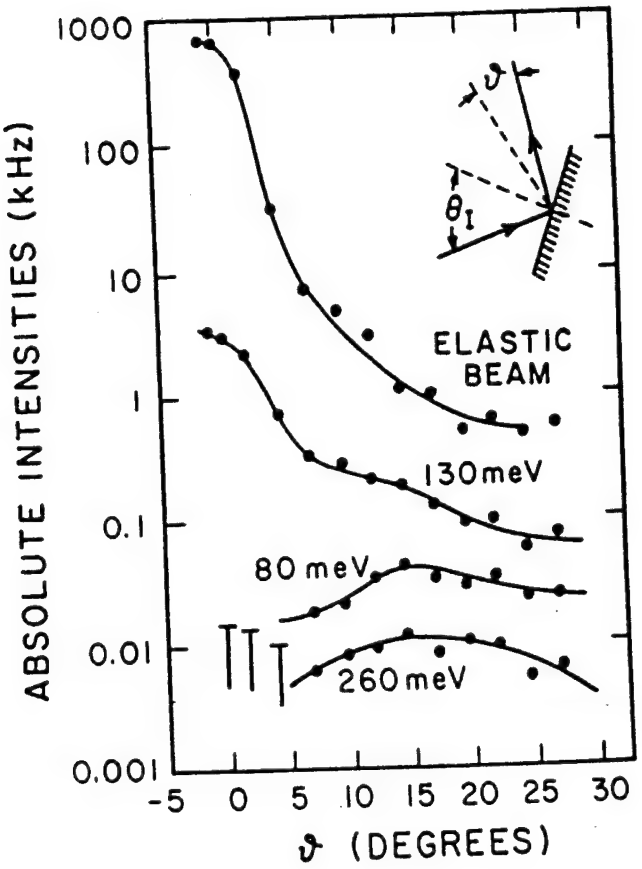

be required. HREELS is an extremely sensitive technique. The limit of detection for strong dipole scatterers such as CO can be as low as 0.0001 monolayer; for weak scatterers such as hydrogen, the limit is 0.01 monolayer. In comparison, IRAS for chemisorbed CO, a strong infrared absorber, is restricted to coverages above 0.1 monolayer. HREELS studies of non-CO organic molecules adsorbed at atomically-smooth electrode surfaces are abundant; similar experiments using IRAS are meager. The energy accessible to HREELS ranges from 100 cm^{-1} to 4000 cm^{-1}; present IRAS detectors are not useful below 600 cm^{-1}. On the other hand, IRAS has higher resolution (nominally 4 cm^{-1}) than HREELS (at best 30 cm^{-1}) and can be utilized for experiments under electrochemical conditions [92-99,102,104]. Figure 12 shows a schematic diagram of an HREELS spectrometer [105]. The energy of incident electrons can be varied from 1 to 10 eV. To afford high resolution, energy monochromation and analysis are done either with a CMA, cylindrical deflector, or spherical deflector analyzers in combination with retarding field optics. Off-specular collection of the backscattered electrons is afforded by rotation of either the sample or the analyzer. Due to extremely low signals (10^{-10} A), continuous dynode electron multiplier detectors have been recommended.

(vii) Work Function Measurements. The work function of a uniform crystal surface is the work to remove a Fermi-level electron from the bulk to the vacuum just outside the surface. This quantity is really a difference in electrochemical potentials of the electron in two places. In the bulk metal the electron has an electrochemical potential $\overline{\mu}_e$ which is equal to the Fermi energy [106,107]. Once the electron is removed to outside the crystal and is at rest, its electrochemical potential has no entropy component and is just the electrostatic potential energy $-e\Phi_o$. Here Φ_o is the electrostatic potential just outside the surface, by which is meant far enough away from the surface that the electron does not feel its image charge. Thus the work function is defined by [106]:

Fig. 12. Schematic drawing of a tandem cylindrical deflector spectrometer used for HREELS. Reproduced with permission [105].

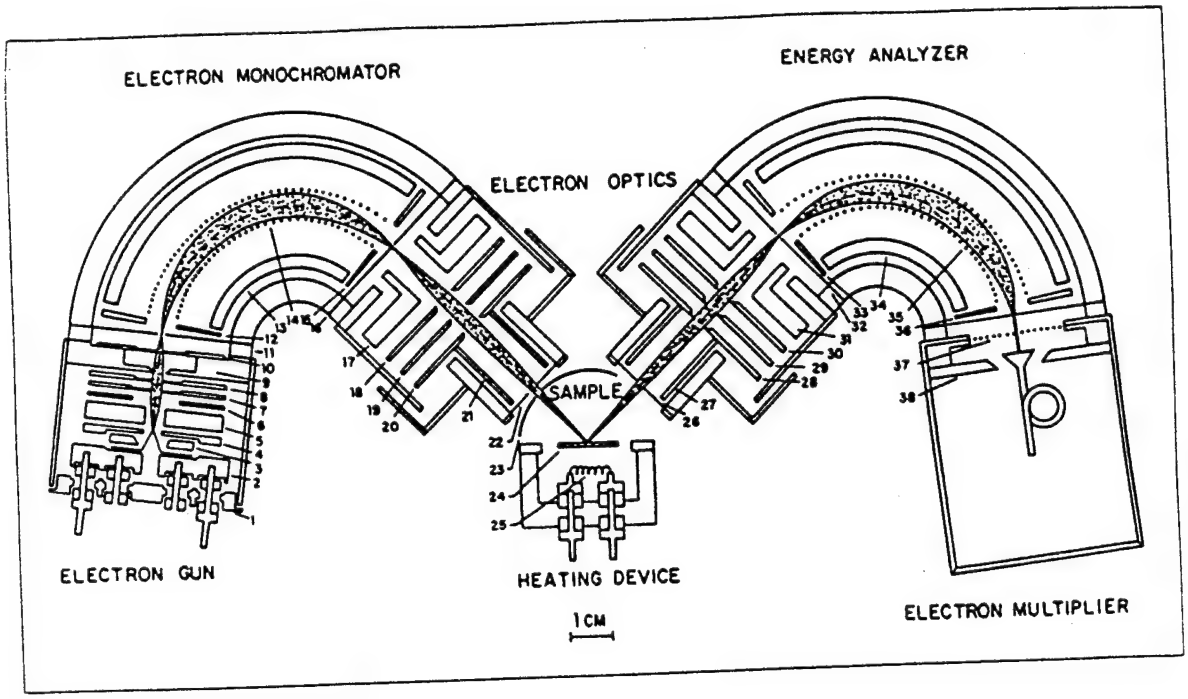

$$\phi = -e\Phi_0 - \overline{\mu_e} = -e(\Phi_0 - \Phi_i) - \mu_e \qquad (3.16)$$

where the second form follows from writing the electrochemical potential as a sum of its chemical (μ_e) and electrical ($-e\Phi_i$) parts. In the second form the bulk contribution μ_e is clearly separated from the surface contribution $e(\Phi - \Phi_i)$. Note that the Fermi energy (or equivalently the electrochemical potential) is not a property only of the bulk, because it contains the electrostatic potential Φ_i inside the metal, which is determined by the surface dipole layers.

In surface adsorption studies, only the surface dipole part $e(\Phi_0 - \Phi_i)$ changes, and consequently the change in work function is equal to the change in this quantity; absolute work functions are less important. For a clean metal surface, the exponential decay of the wave function into the vacuum (electron "overspill") creates the surface double layer. The dipole has the negative end outward, and is dependent on the surface crystallography.

The adsorption of an electronegative atom such as oxygen changes the surface dipole, making the outside of the crystal more negative, and thus increasing the work function. Conversely, an electropositive adsorbate such as Cs increases the work function. For atomic adsorbates, the sign of $\Delta\phi$ is therefore correlated with the direction of charge transfer: positive $\Delta\phi$ is associated with adsorbate to substrate charge transfer and negative $\Delta\phi$ with substrate to adsorbate charge transfer. This reasoning regarding charge transfer has been extended to the case of molecular adsorbates. It should be used with caution, however, because the permanent dipole moment of the molecule is typically a more important contributor to $\Delta\phi$ than the surface chemical bond. The work function also contains potential information about the orientation of the adsorbed molecule, since it probes only the component of the dipole moment normal to the surface.

Drawing quantitative conclusions about adsorbate structure and bonding

from work function measurements is difficult, for several reasons. The work function change is often not proportional to the number of adsorbed molecules, except at low coverages. Accordingly, it reflects not only the properties of individual molecules, but also their interactions; the surface dipoles mutually depolarize one another. Even at low coverages, the dipole moments of adsorbed molecules estimated from $\Delta\phi$ are often much smaller than gas phase dipole moments. Subtle effects of the energy levels involved in the bonding may also be significant, as evidenced by some systems in which even the sign of $\Delta\phi$ is dependent on the type of adsorption site.

Nonetheless, work function measurements lead to useful qualitative conclusions, and empirical correlations between $\Delta\phi$ and the nature of adsorption have been established [8,11,12]. In studies of the structure of the electrode-electrolyte interface, work function change measurements are invaluable since $\Delta\phi$ is very sensitive to both the charge at the electrode and the geometry of the electrochemical double-layer [106,107]. At a simpler level, work function changes are often used to monitor adsorption. After the $\Delta\phi$-*vs*-coverage relationship is established in a calibration experiment, $\Delta\phi$ may then be used as a sensitive measure of surface coverage. Abrupt changes in the slope of the work function vs coverage relationship are diagnostically useful for changes in the type of adsorption, for example completion of an ordered quarter monolayer structure.

Experimental measurements of ϕ and $\Delta\phi$ have been based upon the diode method, field emission, contact potential difference, and the photoelectric effect [11]; the latter two are more commonly utilized. The photoelectric method, which measures absolute values of the work function, is based upon the determination of the threshold energy $h\nu_0$ for photoelectron ejection; the work function is then calculated from the equation $h\nu_0 = e\phi$. The contact potential difference method, which monitors changes in work function, depends on the measurement of the potential difference between two plates in electrical contact. If one of the plates is

used as a reference of constant work function, $\Delta\phi$ at the other plate is manifested as a change in the contact potential. The most common way of measuring the change in contact potential uses a vibrating tip close to the surface as the reference plate (the Kelvin probe method). In its balanced condition there is an electric-field-free region between the sample and the tip, and no induced alternating current flows in the circuit. Adsorption leads to a momentary field, and an alternating current. Electronic feedback is used to adjust the potential on the sample until the field-free condition again applies. The potential adjustment required is equal to the change in work function. Feedback time constants of less than a second are typical.

(viii) Temperature programmed desorption (TPD) or thermal desorption mass spectrometry (TDMS). Thermal desorption techniques [8,11-13] exploit the fact that species adsorbed on a surface will desorb at a rate which increases with temperature. A study of the temperature-dependence of the desorption rate yields data on desorption energies which, for most cases, lead to information on adsorption binding energy states. Thermal desorption can also be used to obtain surface coverages and, in combination with mass spectrometry, determine the composition of species desorbed from the surface. Thermal desorption is a destructive surface analytical tool although it does not always provide a clean surface after one heating cycle in ultra-high vacuum; at catalytic surfaces, complex organic compounds may decompose to form stable graphitic or carbidic layer upon anaerobic heating.

Temperature-induced desorption methods can be classified according to whether the rise in temperature is fast (flash desorption) or is gradual (TPD). In flash desorption, the desorption rate is much greater than the rate at which desorbed gas is pumped out of the system; in this case, the desorption of a given binding state is marked by a plateau in the pressure-temperature curve. In TPD, the slow heating (desorption) rate allows the evolved gases to be pumped out; as a result, the desorption of a particular binding state appears as a peak instead of a plateau in the desorption curve.

The extraction of the activation energy for desorption E_d from the peak temperature T_p in the TPD curves involves the use of the so-called "Redhead equations" [8,11,108]. The desorption activation energy is related to the heat of adsorption ΔH_{ads} by:

$$E_d = E_a + \Delta H_{ads} \qquad (3.20)$$

where E_a is the activation energy for adsorption. Several instances can be found in which the adsorption is non-activated; for such cases, E_d can be equated to ΔH_{ads}.

Thermal desorption experiments based upon measurement of gas pressures are conceptually simple but the experiments are beset with difficulties, such as selective pumping of gases at rates which vary during desorption as well as outgassing from the various elements of the vacuum system due to radiation from the hot sample, which can invalidate quantitative conclusions. Most of these problems can be circumvented by the use of a mass spectrometer to monitor species emitted from the surface. A comparatively inexpensive means for mass spectrometric detection is afforded by a quadrupole mass analyzer, a schematic diagram of which is shown in Figure 13 [109]. This mass filter consists of four parallel rod-shaped electrodes arranged at the apices of a diamond. The existence of an appropriately varying electrical field between the pairs of opposite electrodes will cause all ions to impact on the rods during transit except those of a particular mass-to-charge ratio m/z. Time-of-flight mass spectrometers are more widely used in laser-induced desorption studies.

In TDMS, the substrate is positioned as close as possible to the mass spectrometer; provisions must be made to minimize temperature gradients at the sample surface. The temperature is monitored by a thermocouple wire placed in direct contact with the crystal. Problems associated with degassing from parts of the sample manipulator close to the crystal can be solved by masking the mass

Fig. 13. Schematic diagram of a quadrupole mass filter. Ions B and C have incorrect m/z ratio and are thrown against the rods; A has the proper m/z ratio and is transmitted through the rods onto the detector. Reproduced with permission [109].

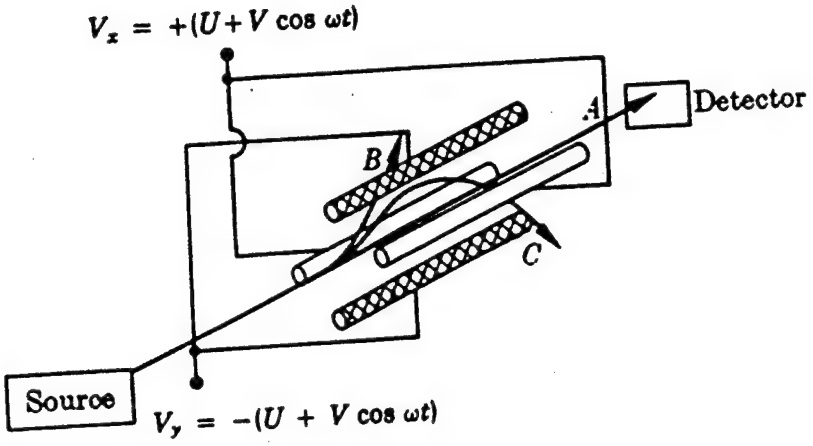

spectrometer with a small aperture such that only line-of-sight detection is possible. For programmed TDMS, microprocessor control allows multiplexed or simultaneous data acquisition of several pre-selected masses.

C. Instrumentation designs

The most critical step in UHV-EC experiments is the transfer of the electrode between the electrochemical cell (at ambient pressures) and the surface analysis chamber (in ultra-high vacuum). Ideally, the transfer is not accompanied by changes in surface structure and/or composition. The simplest approach, which would not require a dedicated surface analysis instrument, is the transfer of the sample electrode through air [110]; clearly this procedure is applicable only if the surface is inert (such as some oxide films) or is covered with a protective film (of solvent or electrolyte) that is removed by evacuation inside the high-vacuum chamber.

The approach employed most successfully in UHV-EC studies of single-crystal electrode surfaces involves the fabrication of a multi-technique surface-analysis apparatus to which an electrochemistry chamber is physically appended. The entire assembly is constructed of stainless steel and can be baked to about 200°C in UHV to attain ultra-clean conditions. Ultra-high vacuum is maintained by a combination of a titanium sublimation pump and either an ion-pump, turbomolecular pump, or a liquid-nitrogen-trapped diffusion pump. Transfer of the electrode between the analysis and electrochemistry chambers is accomplished by a sample manipulator-translator. In some instruments, the crystal remains attached to the same sample holder as it is moved between the two compartments; in other systems, the crystal has to be transferred between two different manipulators. A gate valve isolates the electrochemistry compartment, whenever necessary, from the rest of the system. It is preferable to keep the electrochemistry chamber under UHV when not in use in order to preserve its cleanliness. The electrochemical cell itself is

located inside a bellows-enclosed compartment separated from the electrochemistry chamber by another gate valve; the cell is inserted only after the electrochemistry chamber is brought to ambient pressures with ultra-high purity inert gas. Based upon these considerations, various types of UHV-EC instruments have been constructed [22-28,54,111-116]; two of these are shown for illustrative purposes in Figures 14 and 15.

A typical UHV-EC experiment following instrument bakeout (at which point the base pressure should be less than 5×10^{-10} mbar) would include the following steps. After electrode preparation and initial surface characterization, the electrode is transferred into the electrochemistry chamber which is then isolated from the UHV system, by closure of the appropriate gate valve, and backfilled with high-purity inert gas. The external gate valve is opened and the electrochemical cell is inserted into the chamber. After completion of the electrochemical experiments, the cell is retracted, the external gate valve is closed, and the chamber is pumped down by a turbomolecular or liquid-helium cryogenic pump to less than 10^{-6} mbar. At this point, the main gate valve can be opened to complete the evacuation of the electrochemical chamber and to transfer the electrode into the surface analysis compartment. Pumpdown from ambient pressure to 10^{-8} mbar vacuum can be achieved in less than 15 minutes.

In some UHV-EC designs, an isolable, differentially pumped antechamber is situated between the UHV and electrochemistry compartments. The main function of this antechamber is to minimize the influx of solvent and/or electrolyte vapor into the surface analysis compartment. In this context, it is important to mention that the pressure in the EC chamber is usually an order of magnitude higher than in the UHV chamber; mass spectrometric analysis of the residual gas has revealed that the pressure difference arises primarily from higher amounts of water in the electrochemistry compartment [52]. Because water is only weakly surface-active, it is generally not of major concern in UHV-EC studies. However, in the presence of

Fig. 14. Schematic drawing of an experimental arrangement for UHV-EC studies. In this design, the crystal remains attached to only one sample manipulator. Reproduced with permission [23].

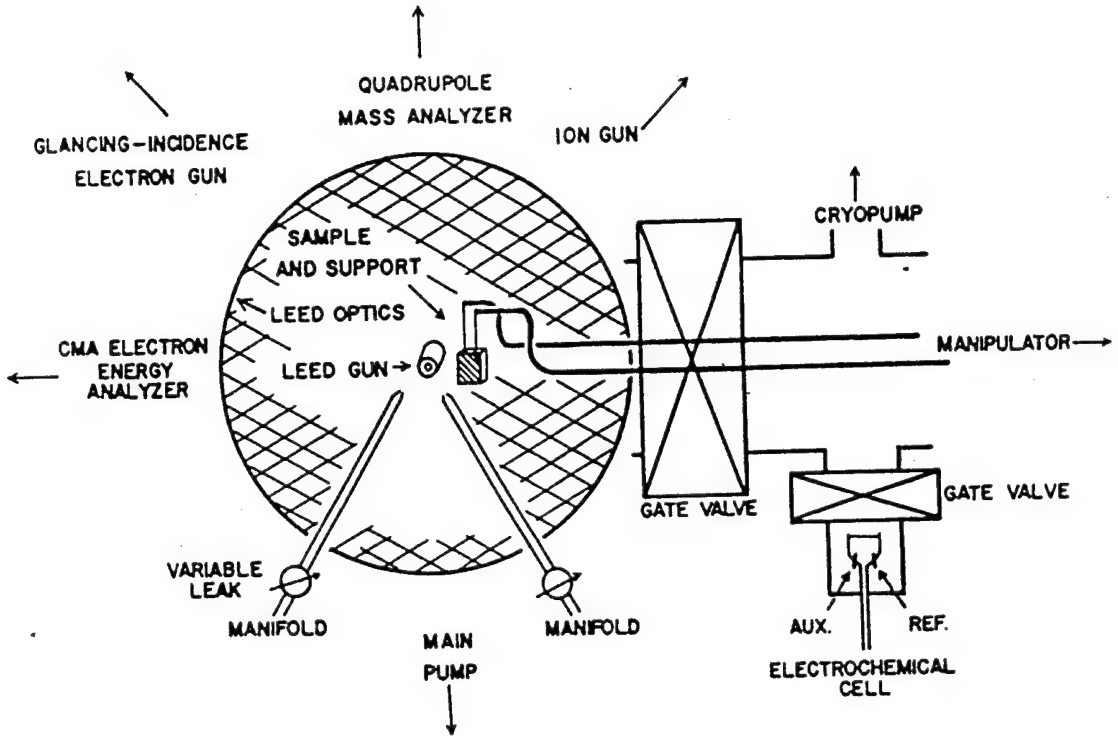

Fig. 15. Schematic drawing of an experimental arrangement for UHV-EC studies. In this design, the electrode is transferred between different manipulators. Reproduced with permission [111]. 85

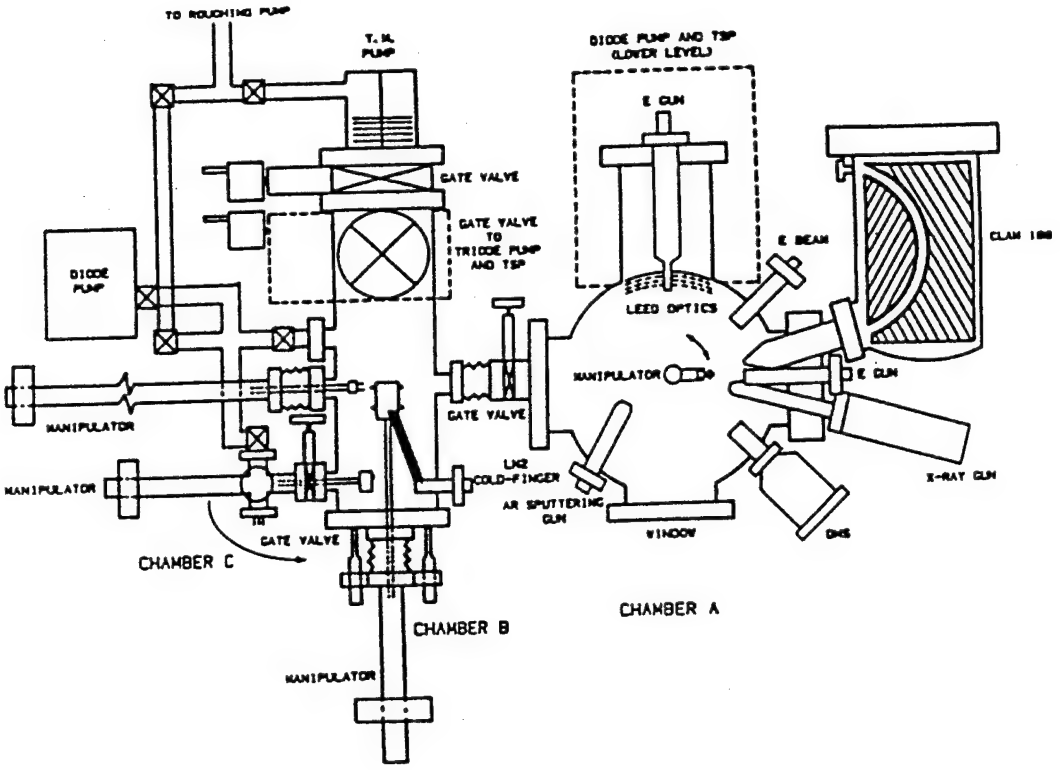

comparatively high quantities of water, impurity species may be dislodged from the walls of the chamber and onto the sample surface. Similar "knock-off" effects can arise when the chamber is backfilled with high purity inert gas. Hence, it is critical to maximize the cleanliness of the electrochemistry chamber and its associated manifold; this can be accomplished by frequent bakeout and continuous evacuation of the electrochemistry chamber when it is not in use.

It is also important to ensure that the backfill gas is of the highest purity to minimize surface contamination by trace-level impurities; argon of at least 99.99% purity is usually employed. Background contamination is metal specific; for example, Cu is more sensitive to residual O_2 while Pt is more susceptible to carbonaceous impurities. Hence, depending upon the nature of the investigation, it may be necessary to pass the high-purity inert gas through molecular scavengers such as a Ti sponge heated to 900°C [52] for still further purification. While efforts to ensure the cleanliness of the UHV-EC system cannot be overemphasized, it must also be realized that electrode-surface contamination can also result from trace-level impurities in the electrolyte solution. Such impurities can originate from the solvent, electrolyte, glassware, and/or the inert gas employed for solution deaeration. The level of solution-based impurities can be minimized by the use of highly purified chemical reagents and gases; in the case of aqueous solutions, the utilization of pyrolytically triply distilled water is recommended [117], although the use of Millipore Milli-Q water is now an acceptable alternative.

Electrochemical experiments have been performed with cells either in the standard or thin-layer arrangement. The latter significantly reduces the level of surface contamination from solution-borne impurities. If the entire electrode is to be immersed in solution, all faces of the single-crystal should be oriented identically in order to obtain characteristic voltammetry. As an alternative, the electrode can be positioned on top of the electrochemical cell in such a way that only one crystal face is exposed to solution, as illustrated in Figure 16. Such a configuration, however,

Fig. 16. Schematic view of an electrochemical cell for use with a single-crystal disc electrode. Reproduced with permission [116].

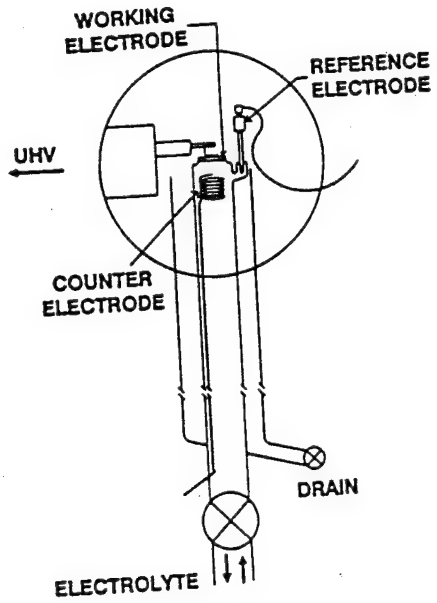

often results in the adherence of a droplet of electrolyte when the electrode is withdrawn from the solution; this problem, on the other hand, does not arise when the electrode is withdrawn slowly (1 mm/sec) in the vertical position [26].

3. FUNDAMENTAL ASPECTS

A. The emersion process

It is important to determine the changes in the interfacial properties when the electrode is removed, at a given potential, from the electrolyte solution. The electrode-withdrawal process under potential control is termed *emersion*. In the ideal process, the emersed electrode retains an interfacial layer identical in composition and structure to that present when the electrode was still in solution. Under electrochemical conditions, the electrode-solution interface is a structured assembly of solvent, electrolyte, and reactant. In the traditional view, this ensemble, commonly referred to as the electrochemical double layer, is subdivided into an inner (compact) layer consisting of field-oriented adsorbed solvent molecules and *specifically* adsorbed anions, and an outer layer composed of solvated cations. The locus of the centers of the adsorbed anions delineates the so-called the inner Helmholtz plane (IHP), whereas the line of centers of the nearest solvated cations defines the outer Helmholtz plane (OHP). Charge transfer reactions of electroactive species are thought to occur at this outer (reaction) plane. The solvated ions interact with the charged metal only through long-range electrostatic forces and, because of thermal agitation in the solution, are distributed in a three-dimensional region that extends from the OHP into the bulk of the solution. This region is identified as the *diffuse layer*, and its thickness is a function of electrolyte concentration; it is less than 300 Å for concentrations greater than 10^{-2} M. Clearly, the electrode-withdrawal process involves a delicate balance with respect to the thickness of the emersion layer: it must be sufficiently thick to incorporate the intact electrochemical double layer but it should also be thin enough to exclude *residual*

(bulk) electrolyte. The electrochemical double layer can, under appropriate electrolyte concentrations, be retained intact when the electrode is withdrawn from solution under potential control. The optimum concentration depends upon whether emersion is hydrophobic or hydrophilic [106,107,118-123]. For the latter type, a thin film of electrolyte adheres to the emerging surface and, consequently, the concentration must not be much higher than 10^{-3} *M* if contamination of the surface by electrolyte ions is not to occur. For hydrophobic surfaces, only the compact layer is retained, and the bulk electrolyte concentration is less important from the point of view of contamination; nonetheless, double-layer discharge is a problem if the concentration is much lower than 10^{-3} *M* since not enough diffuse-layer counterions may be retained. In cases where the mode of emersion is not known, an electrolyte concentration of 10^{-3} *M* appears to be a logical choice.

Investigations of hydrophobic emersion based upon electrode resistance measurements [121], electroreflectance spectroscopy [118,119,122], XPS [123], and work function change determinations [106,107,120] have been able to: (i) demonstrate the existence of an emersed double layer, (ii) determine its stability, and (iii) monitor changes in its structure and composition brought about by the emersion process. The evidence has been compelling that the structure and composition of the double layer in the emersed phase are very similar, if not identical, to those in the solution state; that is, only little or no double-layer discharge occurs upon emersion. More recent studies have focused on the effect of the emersion process on the structure of adsorbed molecular species. Experiments using *in situ* IRAS [124,125] and surface-enhanced Raman spectroscopy (SERS) [126,127] have provided data which demonstrate that the structure and orientation of molecular adsorbates at electrode surfaces are essentially unperturbed by the emersion process.

Upon emersion, the intact double layer loses electrical contact with the bulk electrolyte but not with the electrode. Hence, the overall charge within the interface

must remain neutral. This requirement for neutrality, however, does not disallow the occurrence of spontaneous faradaic reactions within the emersed layer. Such reactions can take place spontaneously provided they do not result in charge imbalance within the layer, even if they are accompanied by loss of material. They consist of redox reactions in which electrons cross the interface, but no net current flows due to the open-circuit conditions. One example is the spontaneous oxidation of electrodeposited Cd in aqueous media:

$$Cd_{(s)} + 2H_2O \rightarrow Cd(OH)_{2(s)} + H_{2(g)} \qquad (4.3)$$

In this reaction, the water is from either the diffuse layer or the residual gas in the UHV chamber.

B. Perturbations caused by evacuation and surface analysis

Another critical issue in coupled UHV-EC experiments pertains to perturbations of the emersed double layer caused by the evacuation and surface analytical processes. Alterations in the surface electronic structure can be studied by work function change measurements; representative results are shown in Figure 17 in which a plot of the work function of a polycrystalline Au emersed from 0.1 *M* $HClO_4$ into UHV as a function of the emersion potential is presented [107,128]. It can be seen here that the work function tracks the applied potential over a wide range, even into the oxide formation region. This, and other sets of data demonstrates that the electronic properties of the double layer are unaffected by emersion either into the ambient or into UHV. Recent comparisons of emersion work function changes with absolute electrode potential suggest that some water molecules may reorient upon emersion [129].

An expected effect of evacuation is the change in the composition within the electrochemical double layer by UHV-induced desorption; the extent of the

Fig. 17. Work function as a function of emersion potential of polycrystalline Au emersed from 0.1 *M* $HClO_4$. The work function of the clean metal was 5.2 eV. The lower and upper lines, respectively, represent the solution inner potential if the absolute NHE half-cell potential is 4.45 or 4.85 V. Reproduced with permission [107].

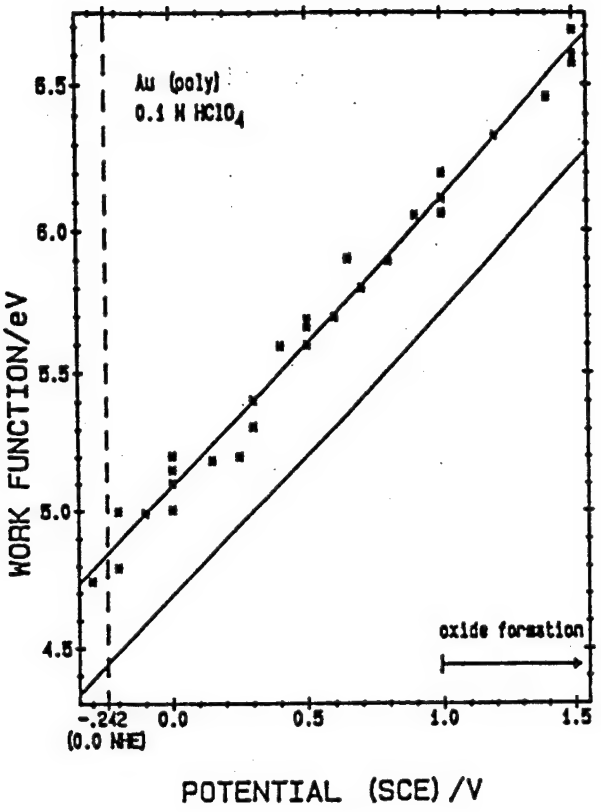

compositional changes will depend primarily upon the heats of vaporization ΔH_{vap} or sublimation ΔH_{sub} of the *unbound* materials entrapped within the emersed layer. Obviously, excess water, unadsorbed gases, liquids, and sublimable solids will be removed readily in UHV. Water retained as part of the hydration sphere of the counter cations can survive the evacuation process if the hydration enthalpies ΔH_{hyd} are substantial [75,130,131].

Adsorbed species with ΔH_{ads} well in excess of 40 kJ mole^{-1} are expected to be unaffected by exposure to ultra-high vacuum. Counterions retained in the diffuse layer would also be stable in vacuum unless they undergo solvolysis reactions which would be enhanced at very low pressures; an example is provided by the hydrolysis of HCO_3^-:

$$HCO_3^- \rightarrow OH^- + CO_{2(g)} \qquad (4.4)$$

Strongly chemisorbed species, such as iodine at the noble-metal electrodes, are expected to form stable well-ordered adlattices in solution [61,85] that would not reconstruct in vacuum. Similarly, the surface coverages and molecular structures of chemisorbed molecules are expected to withstand the evacuation process. One example is provided by 3-pyridylhydroquinone (Py-H_2Q) which is chemisorbed on a Pt(111) electrode surface through the N-heteroatom [132]. In such a mode of surface attachment, the diphenol group is pendant and able to undergo the following reversible quinone/hydroquinone redox reaction:

$$Pt(111)\text{-}Py\text{-}Q + 2e^- + 2H^+ \leftrightarrow Pt(111)\text{-}Py\text{-}H_2Q \qquad (4.5)$$

where Q and H_2Q, respectively, represent the pendant quinone and hydroquinone groups. Figure 18 shows cyclic voltammetric curves that correspond to Reaction (4.5) for chemisorbed Py-H_2Q before and after a one-hour exposure to UHV. It is

Fig. 18. Cyclic voltammetry of 3-pyridylhydroquinone at Pt(111). (A) Solid curve: first scan; dotted curve: after 1 hour in UHV. (B) Solid curve: first scan; dotted curve: second scan. Reproduced with permission [132].

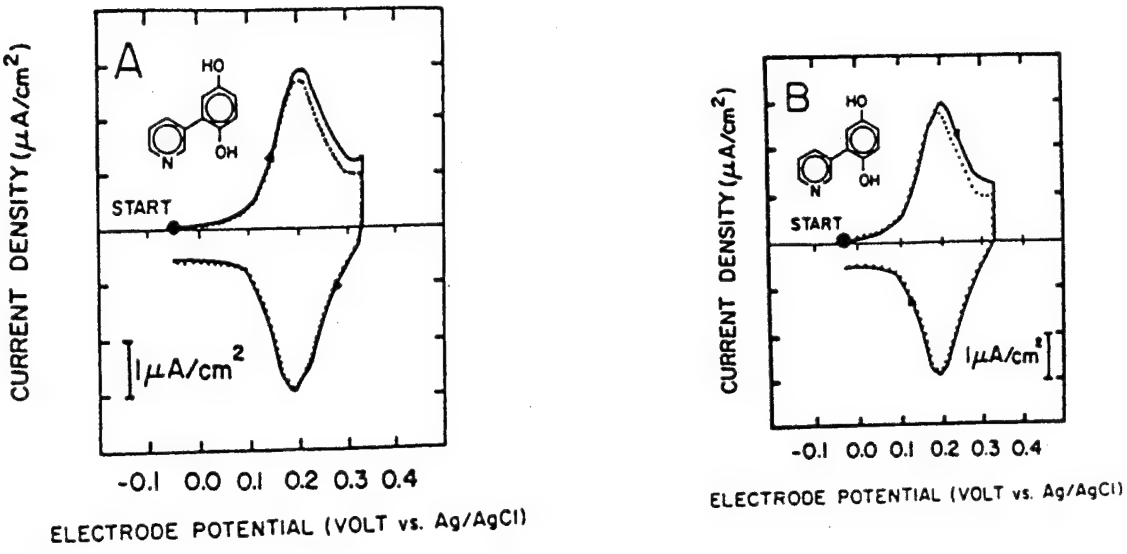

clear from the data presented that the reversible electrochemical reactivity of the chemisorbed layer has not been affected by the prolonged exposure to UHV.

Perturbations can also arise from the surface characterization method itself. For example, the extraction of ΔH_{ads} information from TPD is based upon the measurement of the desorption energy E_d; implicit in the technique is the requirement for complete desorption. Hence, by its very nature, TPD is a totally destructive technique. On the other hand, surface analytical methods based upon electron and optical spectroscopies are not intended to damage the surface layer; nevertheless, beam damage is common in these methods. Unless exceedingly high photon fluxes are used, optical methods are non-deleterious relative to particle-based techniques.

Several surface processes are known to be stimulated by electron impact. Examples are binding-site conversions, dissociative chemisorption, and particle desorption [11]. Such processes take place even at very low electron power densities (minimal sample heating), which signifies that surface thermal effects are insignificant. The possibility of stimulation by momentum transfer can be assessed by noting that the maximum kinetic energy ΔE transferred to a particle of mass M upon collision with an electron of mass m_e and kinetic energy E_e is relatively small [11]:

$$\Delta E \approx 4E_e m_e/M \tag{4.6}$$

As an example, the maximum energy imparted by an electron of 300-eV energy would be 0.3 eV to an adsorbed H atom; in comparison, the adsorption enthalpy of strongly bound hydrogen is greater than 2 eV. Hence, for low-energy electrons, momentum transfer events cannot cause significant structural and compositional changes in the emersed layer. It is now accepted that electron-stimulated reactions occur mainly via electronic excitations. These excitations can lead to bond

dissociation and form the basis of the surface spectroscopic technique known as electron stimulated desorption ion angular distribution (ESDIAD) [133].

Pendant functional groups not directly bonded to the substrate surface, such as the diphenol moiety in Py-H_2Q, are most prone to electron-stimulated desorption. In other instances, electron irradiation can induce surface displacement reactions that involve species present as residual gas in the analysis chamber. However, it is essential to note that the electron-stimulated alterations would be detrimental only if the post-analysis layers are to be used for further electrochemical experiments. In those rare instances when additional experiments have to be performed, it is a simple matter to regenerate the surface to exactly the point just prior the surface analysis. Beam damage can be assessed by repeated analysis over a period of time followed by extrapolation of the data to *zero* time.

4. CASE STUDIES

UHV-EC investigations with *single-crystal* electrode surfaces can be broadly classified into three groups. The first places emphasis on the structure and constitution of the electrochemical double layer as functions of electrode potential and solution composition. The second centers on electrodeposition reactions; included in this category are extensive studies on hydrogen and oxygen adsorption at platinum electrodes. The third deals with the interfacial structure and reactivity of chemisorbed complex molecules.

A. Electrochemical Double Layer

Two general strategies have been adopted in UHV-EC studies of the electrical double layer. One, strictly a model approach, involves the synthesis of the double layer in UHV by sequential cryogenic adsorption of its constituents [134-140]; the temperature must be maintained below 160 K at all times in order to prevent the evaporation of unbound solvent. The other approach is based upon the structural

and compositional analysis of the emersed layer; since surface characterization is done at ambient temperatures, excess water in the diffuse layer is pumped away.

The viability of the cryogenic coadsorption approach was tested by comparison of work-function changes $\Delta\varphi$ for UHV-synthesized and electrochemical Ag(110)-X-H_2O layers, where X denotes Cl^- or Br^- [134-138]. The results showed that there is good agreement between the UHV and *in situ* results, provided that *coadsorbed* water is present in the UHV-generated layer. The satisfactory agreement indicates that, at least under zero diffuse-layer charge conditions, microscopic-level information from the UHV simulation work is relevant to electrochemical systems despite the large temperature difference. The requirement of solvation implies that the electronic properties of the unsolvated Ag(110)-Br interface are quite different from those of the fully solvated Ag(110)-Br-H_2O layer. Other more complex interfacial systems have also been modeled via cryogenic coadsorption. For example, UHV-synthesized H_2O-HF-CO coadsorbed layers were studied at Pt(111) and Rh(111) surfaces by HREELS, LEED, TPD and XPS [139,140]. In that work, the "control" of electrode potential was based upon coadsorption of H_2. The cryogenic coadsorption approach to the study of the electrochemical double layer offers two main advantages [139,140]: (i) the control of interfacial parameters far more precisely than can be achieved in solution, and (ii) the detailed characterization of fully solvated species by a host of complementary surface-sensitive spectroscopic methods. Still, it must be realized that this approach provides only models, the relevance of which to electrochemistry remains to be fully established.

The direct approach to the study of the electrochemical double layer involves the surface characterization of the electrolyte layer retained at the electrode surface as it is withdrawn from solution. Although the direct approach is more realistic than the UHV simulation strategy, it is applicable only to cases in which the compact layer consists of materials which, because they are either strongly adsorbed

or in the solid-state, remain on the surface when evacuated to UHV. It is also implied in this approach that those solvent molecules pumped away are inconsequential in the formation and preservation of the electrochemical double layer. This is not an unreasonable premise since chemisorption involves strong chemical interactions that are only be minimally perturbed by physisorbed species.

UHV-EC studies of the interaction of electrode surfaces with anionic electrolyte have been carried out at well-defined Pt(111) [75,130,131,141-145], Pt(100) [146,147], stepped Pt(s)[6(111)×(111)] [148], Cu(111) [113,149], Ag(111) [150] Au(111) [151], and Pd(111) [42-44,85,152] electrodes; all these studies have been with aqueous solvents. The anions studied include monatomic species such as Cl^- [142,146,147,150], Br^- [141,146,147,150], I^- [42-44,85,143,150,153,154], and SH^- [144,152], and polyatomic species such as CN^- [75,130,131], SCN^- [131], and SO_4^{2-} [149,155]. All of these anions yield surface coverages and well-ordered structures that depend upon the solution pH and the applied potential.

B. Underpotential electrodeposition

The cathodic electrodeposition of *submonolayer* quantities of one metal onto another generally occurs at potentials positive of that for *bulk* deposition because of preferential interactions between the substrate and the foreign-metal electrodeposit. This underpotential deposition (UPD) process is strongly influenced by the structure and composition of the substrate; hence, UPD research is one in which UHV-EC methods have been extremely valuable. UHV-EC studies of UPD can be categorized according to whether the experiments were used to correlate the substrate structure with the electrodeposition voltammograms or to determine the resultant interfacial properties of the adatom-modified substrate. Investigations devoted to structure-voltammetry correlations help establish reference states which new experiments can be calibrated against; those focused on post-deposition characterization yield information concerning the electrocatalytic selectivity of the

mixed-metal interfaces.

The first applications of LEED and AES in electrochemistry involved the correlation of the surface crystallographic orientation with the underpotential hydrogen deposition at Pt electrodes [48]. Those studies were motivated by earlier work with polycrystalline Pt electrodes whose cyclic voltammograms showed two hydrogen deposition peaks. These studies, however, were not judged to be definitive because of the lack of a rigorous control of substrate structure, and the use of multiple surface oxidation-reduction cycles to generate a clean, *but structurally disordered*, surfaces. Nevertheless, they provided the impetus for further adaptation of UHV-based surface structural tools to interfacial electrochemistry.

Later studies based upon *non*-UHV-prepared single-crystal surfaces led to the discovery of new voltammetric features for Pt(111) in the form of highly reversible pseudocapacitance peaks at potentials *well positive* of the usual hydrogen deposition peaks [32,47-49,156]. These peaks can be seen when the Pt(111) voltammograms in H_2SO_4 and $HClO_4$ are compared for a flame-annealed sample with those for a UHV-prepared (but electrochemically cycled) electrode. Verification studies employing UHV-EC instrumentation equipped with improved vacuum-to-electrochemistry transfer technology were able to reproduce the new voltammetric results. Extensive follow-up *in situ* and UHV-EC work then ensued which clarified several aspects of this exceedingly surface-sensitive reaction [47-49,155].

A few investigations have been carried out on the formation of underpotential states of oxygen. Electrochemical experiments have been performed only with Pt(100) and Pt($11\bar{1}$) electrodes [24,157-159]. Gas-phase and solution-state reactions with oxygenous species have been carried out at stainless steel single crystals [160-162]. The occurrence of place-exchange during anodic film formation has been studied via LEED spot-profile analysis [24,159]. This irreversible place-exchange reaction accounts for the common observation that the electrode surface loses its single crystallinity even after minimal surface oxidation.

The literature on monolayer metal deposits is extensive. Most of the work pertains to the geometric, electronic, and catalytic properties of foreign metals *vapor deposited in UHV* onto single-crystal substrates; a compilation of the adlattice structures of such metal adlattices has been published [163]. Studies of foreign metal monolayers *deposited electrochemically* have been primarily with polycrystalline substrates. The first UHV-based investigation of electrochemically deposited admetals employed XPS to determine the core-level shifts of submonolayer Cu and Ag on *polycrystalline* Pt [164,165].

The first UHV-EC work on electrodeposition at well-defined electrode surfaces involved Ag at an iodine-coated Pt(111) electrode [166,167]. The iodine pretreatment was done in UHV to form a protective Pt(111)($\sqrt{7}\times\sqrt{7}$)R19.1°-I adlattice before immersion into a solution containing dilute Ag^+ in 1 *M* $HClO_4$. Subsequent studies included Ag electrodeposition on I-coated Pt(100) [168] and stepped Pt(s)[6(111)×(111)] [35], Cu on I-pretreated Pt(111) [169], and Pb on I-covered Pt(111) [173]. Sn [171] and Pb [172] deposition onto *iodine-free* Pt(111) in Br^- or Cl^- [173] solutions has also been studied. Although the Pt substrate was not pretreated with I, the presence of halide ions in the plating solution led to specific adsorption of anions prior to the deposition process.

Electrodeposition from solutions free of surface-active anions have been studied. These investigations, carried out in ClO_4^- or F^- electrolyte, include UPD of Cu on Pt(111) [174-176], Tl, Pb, Bi, and Cu on Ag(111) [177], and Pb on the three basal planes of Ag [111]. Invariably, the underpotentially deposited films showed unique adlattice geometries that were dependent upon the substrate orientation and the admetal coverage.

The atomic layer epitaxy (ALE) approach to deposition of a compound film, based upon the alternate layer-by-layer deposition of the elements of the compound, has recently been adopted in the electrochemical synthesis of compound semiconductors. This electrochemical analogue, referred to as electrochemical

atomic layer epitaxy (ECALE) [79,178,179], takes advantage of the fact that only monolayer quantities are produced by underpotential deposition. The UPD-based epitaxial growth of CdTe on Au(111) has been monitored by LEED and AES [79].

C. Molecular adsorption

The capability to prepare single-crystal surfaces by thermal treatment at ambient pressures [32,156,180-182] has fostered the proliferation of non-UHV studies of the adsorption of molecules at monocrystalline electrodes. The detail of information obtained from such *in situ* work, however, falls short of that provided by UHV-EC experiments. As one example, although *in situ* IRAS has provided much information about the structure-sensitivity of the chemisorption and anodic oxidation of CO, its sensitivity is too low to permit meaningful investigations with other molecules even as simple as ethylene.

(i) Solvent-electrode interactions. The nature of the interactions between the solvent and the electrode surface has significant ramifications in electrochemical surface science. For instance, the use of strongly surface-active solvents would severely repress electrocatalytic processes that rely on a direct interaction between the reactant and the metal surface. The bonding of water to metal surfaces is an important issue in aqueous electrochemistry. In models suggested to explain the potential dependence of double-layer capacity, the existence has been postulated of monomeric and clustered water molecules, both of which are able to adopt two opposite dipolar orientations with respect to the surface [183,184]. The studies of water adsorption on single-crystal electrodes are all based upon vapor deposition in UHV usually at cryogenic temperatures since water is not adsorbed on clean metal surfaces at ambient temperatures. Of significant interest to electrochemistry is the observation that, on Ni, Pt, Ag, Cu, and Pd, water is dissociatively chemisorbed *if* the surface contains *submonolayer* coverages of oxygen [185]. The reaction is thought to occur by hydrogen abstraction. This reaction is very metal-specific since

at other noble metals such as Ru(001), adsorbed oxygen is inactive towards water dissociation [185]. UHV coadsorption experiments of water and acids also provide useful information on the nature of the interface for some common electrolyte-electrode combinations, such as HF/H_2O on Pt(111) [186] and HNO_3/H_2O on Ag(110) [187]

Nonaqueous solvents commonly used in electrochemistry include acetonitrile, dimethylformamide, *p*-dioxane, sulfolane, dimethylsulfoxide, pyridine, acetic acid, propylene carbonate, liquid ammonia, and dichloromethane [188]. Work involving such materials can be categorized according to whether the electrode is allowed to interact with the nonaqueous solvent by (i) vapor dosing in vacuum, (ii) exposure to aqueous solutions containing small quantities of nonaqueous-solvent material, or (iii) immersion in pure nonaqueous solvent. UHV-EC work of the latter type using single-crystal electrodes has not been pursued, although an XPS study of polycrystalline Li thin-film electrodes immersed in neat acetonitrile has been reported [115]. Studies that employed aqueous solutions containing small amounts of nonaqueous solvent are more abundant; however, such investigations are usually classified under electrode-solute, rather than electrode-solvent, interactions. Except for one case, all UHV-based adsorption studies with nonaqueous-solvent compounds (carboxylates, ammonia, and N-heteroaromatics) were carried out purely in the context of gas-solid surface science [8,189]. The intent of the one exception [190] was to use the reactions between the solvent vapor and the metal surface as models for the electrochemical analogues; for better simulation of solution conditions, vapor dosing was up to $0.\overline{3}$ mbar, approaching the vapor pressures of the liquid solvents.

(ii) Group IB electrodes. Most organic compounds are only weakly adsorbed on Cu, Ag, and Au electrode surfaces; hence, unless the adsorbate itself is a solid or when adsorption is carried out at cryogenic temperatures, meaningful UHV-EC experiments with the coinage metals are limited. One study, which took advantage of the strong interaction of the -SH functional group with the coinage metals, used

HREELS, LEED, AES, and voltammetry to determine the influence of the location of the N heteroatom on the adsorption properties of the isomers 2-mercaptopyridine and 4-mercaptopyridine at Ag(111) in aqueous HF [191]. The subject compounds were postulated to undergo isomerization upon oxidative adsorption through the -SH moiety.

(iii) Group VIII electrodes. The abundance of studies of organic molecular adsorption at electrode surfaces involves the platinum-metals. This is of course not surprising since these metals are well known for their electrocatalytic activities and an immense body of work has already been amassed for these materials in their polycrystalline states [192-197]. Surface electrochemical studies of metal-organic compounds at single-crystal electrodes can be broadly classified according to whether the work was done with CO (and related small molecules) or with more complex molecules. The former are more numerous, although a vast majority of such studies have been carried out *without* UHV-based surface characterization. Work with well-defined surfaces have been limited to LEED of CO adlattices on Pt(111) [198] and Pd(111) [199], and HREELS, LEED, TPD and XPS of mixed H_2O-HF-CO layers generated in UHV by cryogenic adsorption at Pt(111) and Rh(111) surfaces [139,140]. An impressive amount of detailed information on a wide variety of complex organic compounds chemisorbed at well-defined Pt(111) and Pt(100) electrode surfaces has been furnished by LEED, AES, TPD, and HREELS [23,76,200,201]. Electrocatalytic reactivity studies which accompanied these investigations were limited to anodic oxidation reactions, and only correlations between the mode of adsorbate bonding and extent of anodic oxidation were attempted.

(a) Carbon monoxide. Much of what is known about the structure and reactivity of CO chemisorbed at single-crystal electrodes, and their dependencies on surface crystallographic orientation, electrode potential, and adsorbate coverage are based almost entirely upon *in situ* IRAS measurements [182]. Only a few UHV-EC

studies on CO have been reported. One made use of a well-defined Pt(111) surface and sought to correlate anodic peak potentials with observed LEED structures [198]. A later study examined the lateral modification and re-organization of the CO adlattice brought about by coadsorbed I [202]; compression of the CO domain by I was postulated. Another study based upon LEED, AES, TPD, voltammetry, and coulometry, examined the chemisorption of CO at well-defined and anodically disordered Pd(111) [199]: It was shown that CO adsorption from solution yielded an ordered adlattice, Pd(111)c(4×2)-CO, in which the CO molecules occupy two-fold hollow sites; at the oxidatively disordered surface, CO chemisorption occurred spontaneously but no ordered CO adlayers were produced which was taken as an indication that the CO molecules resided on atop sites; Pd(111)c(4×2)-CO yielded two oxidation peaks the first of which was accompanied by an adlattice reconstruction from c(4×2) to (√3×√3)R30° (Figure 19). The electrochemical oxidation of UHV-prepared Ni(111)-c(4×2)-CO in alkaline electrolyte has recently been investigated [203]; it was determined that the CO adlayer remains intact up to the moment of contact with the electrolyte and can be electrooxidized quantitatively to CO_2.

(b) Other organic compounds. UHV-EC investigations have been undertaken to understand the nature of the chemical interactions between the organic molecule and the electrode surface as a function of interfacial parameters, such as pH and electrode potential, and also to correlate the mode of attachment with the reversible and/or catalytic electrochemistry of these materials.

The differences between gas-phase and solution-state chemisorption and catalytic hydrogenation of ethylene have been documented [204]: variations in the structures of ethylene chemisorbed at the solid-solution and gas-solid interfaces lead to different reaction pathways. In solution, ethylene chemisorption occurs molecularly through its π-electron system, whereas chemisorption in UHV is accompanied by molecular rearrangements to form a surface ethylidyne species. In

Fig. 19. Current-potential curve for the anodic oxidation of CO chemisorbed on Pd(111), initially in the Pd(111)c(4×2)-CO structure. The supporting electrolyte consisted of 0.1 m*M* NaF and 0.1 m*M* NaOH. The shoulder in peak I is due to polycrystalline edge effects. The potential sweep rate was 2 mV/sec.

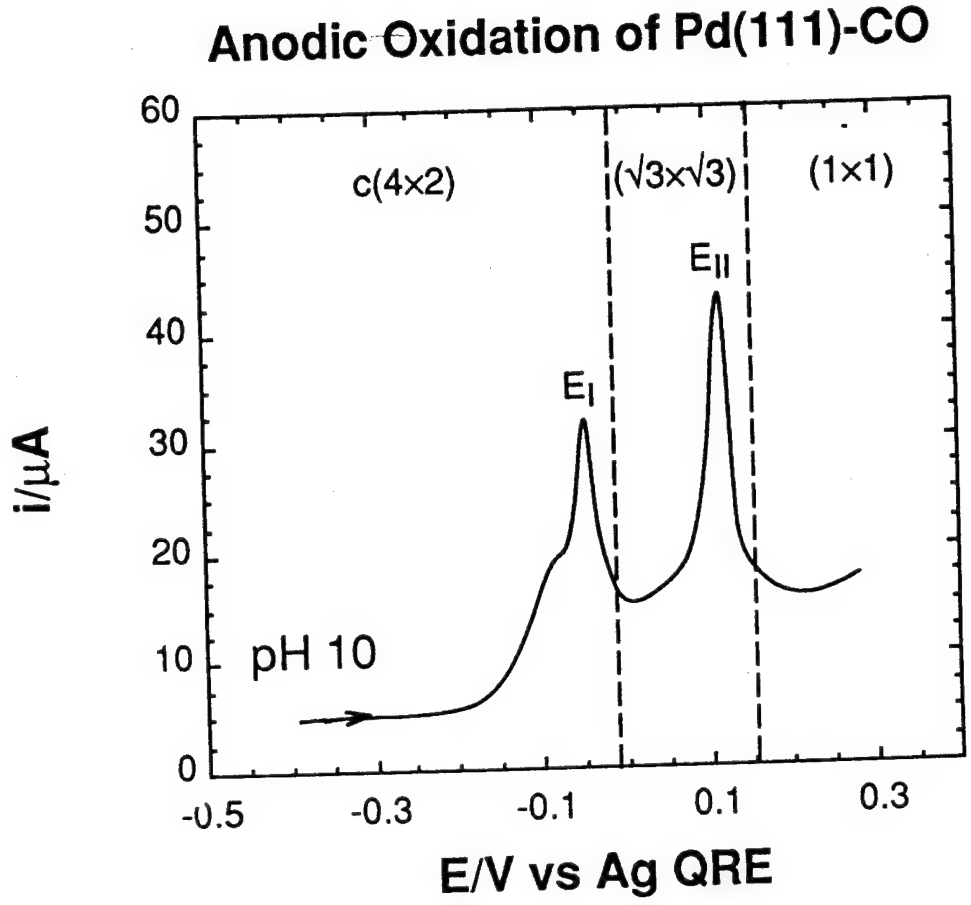

electrocatalytic hydrogenation, ethylene is reduced on the Pt surface by adsorbed H atoms; in gas-phase hydrogenation, H atoms must be transferred from the Pt surface through a layer of irreversibly adsorbed ethylidyne to ethylene adsorbed on top of the ethylidyne layer. Other studies [204-206] compared the electrocatalytic hydrogenation of ethylene at polycrystalline and well-defined Pt(111) and Pt(100) single crystals. Further work with alkenes [207-213] has been focused on the effects of hydrocarbon chain length and the presence of weakly surface-active substituents such as carboxylates [214] and alcohols [215]. These studies showed that: (i) the primary mode of surface coordination of terminal alkenes, alkenols, and alkenoic acids is through the π-electron system of the olefinic double bond; and (ii) the pendant alkyl chain is always extended outward on top of the propylene moiety. This type of coordination is the same for the alkenols and alkenoic acids. Under favorable circumstances, intermolecular hydrogen bonding may occur within the alkenol layer [215], or the carboxylate group may interact directly with the metal surface [214]. From coulometric measurements, it was concluded that electrocatalytic oxidation of the chemisorbed higher alkenes is limited largely to the olefinic anchor [214,215]. Electrochemical oxidation of the lower alkenols, such as allyl alcohol, proceeds to completion yielding only CO_2 and H_2O [214,215]. Evidently, only groups that are in close proximity to the electrode surface undergo anodic oxidation.

Early studies with smooth polycrystalline based upon Pt thin-layer electrochemical techniques and *ex situ* IRAS indicated that aromatic compounds typified by 1,4-dihydroxybenzene (H_2Q) are chemisorbed in discrete, non-random orientations that depend upon interfacial factors such as temperature, concentration and electrolyte coadsorption [216-221]. Experiments implemented with well-defined Pt(111) electrodes , such as the HREELS data shown in Figure 20 for H_2Q adsorbed from low and high concentrations, support the earlier findings although the exact conditions at which the multiple orientational transitions occur

Fig. 20. Specular EELS spectra of adsorbed 1,4-dihydroxybenzene (H2Q) and benzoquinone (BQ) at Pt(111). A: Adsorption from 0.1 m*M* HQ solution. B: From 1.0 m*M* BQ solution. C: From 500 m*M* HQ solution. Reproduced with permission [23].

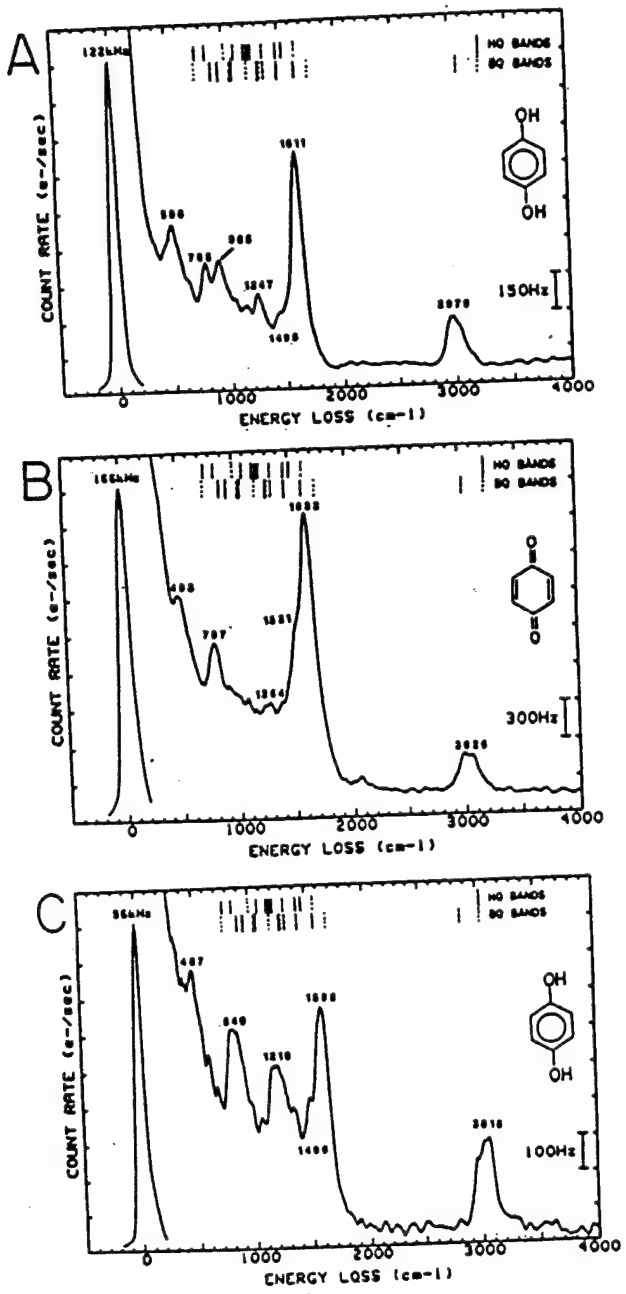

are different for the polycrystalline and single-crystal electrodes [23,75]. The electrocatalytic oxidation of multiply oriented aromatic molecules has been shown to be strongly dependent on their *initial* adsorbed orientations [222-224]. For example, flat-adsorbed hydroquinone is oxidized completely to CO_2, while oxidation of the edge-oriented chemisorbed species is less extensive.

Sulfur-containing compounds investigated included thiophenol, pentafluorothiophenol, 2,3,5,6-tetrafluorothiophenol, 2,3,4,5-tetrafluorothiophenol, 2,5-dihydroxythiophenol, 2,5-dihydroxy-4-methylbenzyl mercaptan, and benzyl mercaptan; chemisorption of these compounds occurs oxidatively through the sulfur group with loss of the sulfhydryl hydrogen [85,195]. The tethered diphenolic moieties in the adsorbed dihydroxythiophenols show reversible quinone/diphenol redox chemistry.

S-heterocyclic compounds studied were thiophene, bithiophene, and their carboxylate and methyl derivatives [225]. Experimental evidence indicates that these compounds are bound exclusively through the S heteroatom, although the chemisorption process is accompanied by desulfurization reactions; the extent of self-desulfurization increases as the adsorption potential is made more positive. The electropolymerization of 3-methylthiophene at clean Pt(111) and monomer-treated Pt(111) pretreated has been studied, and the properties of the two types of polymer film were compared [225]. In terms of the HREELS spectra, two major differences were noted which were attributed to changes in the physical nature of the polymer film, such as swelling or losses in reflectivity, and/or to excitation of phonon modes in the polymer.

The chemisorption of pyridine [226], bipyridine [227], multinitrogen heteroaromatic compounds [228], and their derivatives has been examined as a function of isomerism and substituents. Pyridine forms a well-ordered layer of admolecules chemisorbed through the N heteroatom in a tilted vertical orientation. The derivatives are coordinated similarly unless the ring nitrogen is sterically

hindered such as in 2,6-dimethylpyridine where chemisorption is in the flat orientation via the π-system of the aromatic ring. Pyrazine, pyrimidine, and pyridazine are chemisorbed through only *one* nitrogen heteroatom in a tilted-vertical orientation [228]. For their derivatives, adsorption occurs through the least hindered ring nitrogen. Carboxylate substituents located in positions *ortho* or *meta* to the nitrogen heteroatom interact with the Pt(111) surface at positive potentials, behavior similar to that shown by the corresponding pyridine carboxylates. Figure 21 depicts these different orientations. The chemisorbed layers were disordered as indicated by the absence of LEED patterns and were observed to be electrochemically unreactive. The adsorption behavior of the bipyridyls is also sensitive to steric hindrance at the positions *ortho* to the nitrogen heteroatom [227].

The mode of chemisorption at well-defined Pt(111) of L-dopa, L-tyrosine, L-cysteine, L-phenylalanine, alanine, and dopamine has been studied [229,230]. Except for L-phenylalanine, chemisorption occurs preferentially through the -SH moiety or the aromatic ring. This is as expected from what is known about the relative surface activities of various functional groups at polycrystalline Pt: It has been empirically determined via competitive chemisorption experiments that the strength of adsorption decreases in the order: -SH > hetero N > quinone/diphenol ring > C=C ≥ benzene ring ≥ amine N (pH 7) > -OH > -C=O [220].

Fig. 21. Structural models of 3-pyridinecarboxylate (niacin) chemisorbed at well-defined Pt(111) as functions of pH and electrode potential. Reproduced with permission [226].

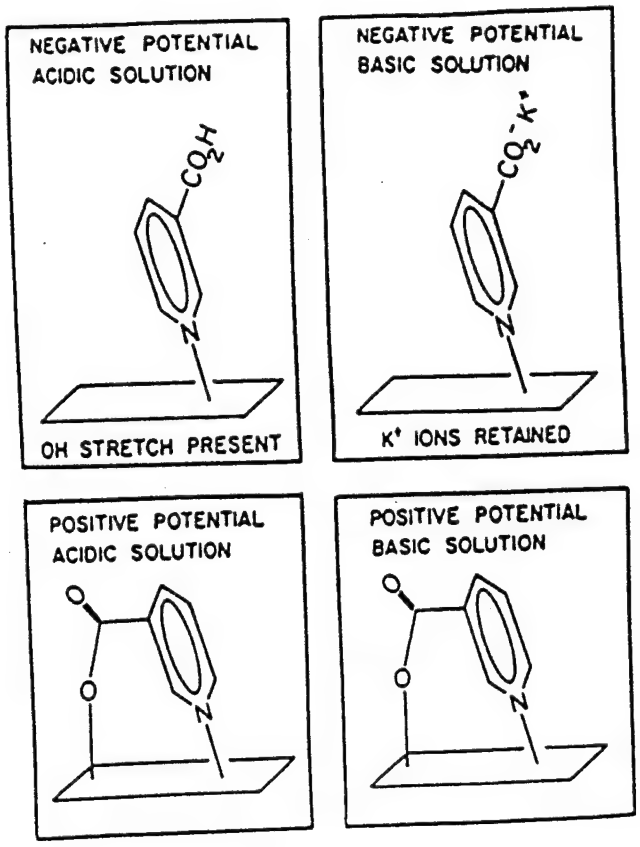

5. SUMMATION

The principal aim of modern electrochemical surface science is the establishment of fundamental correlations between the structure, composition and chemical reactivity at the electrode-solution interface. Such correlations would permit the design of superior electrode materials not only to monitor but also to control important electron-transfer reactions. It is evident from the present review that, because of the new avenues of investigation afforded by UHV-EC techniques, significant advances have been taken in this direction. Experiments can now be designed to determine the identity, electronic structure, molecular configuration, mode of surface coordination, enthalpies of adsorption, and the two-dimensional arrangement of electrocatalytic reaction intermediates. The utilization of UHV methods in interfacial electrochemistry was initially restricted to only a few laboratories, but the number of researchers in the area has grown. It is particularly interesting to note that surface science laboratories which previously devoted efforts solely to gas-solid interfaces now apportion significant time to the study of electrochemical phenomena.

There are three principal functions of coupled UHV-EC experiments: (i) It can be used to prepare unique surfaces of well-defined structure and composition for the performance of specific electrochemical tasks. (ii) It can be employed to determine the structure and composition of the compact layer at the electrode-solution interface. (iii) It can be exploited to monitor the composition and lateral structure of non-specifically-adsorbed materials in the diffuse layer. These tasks will always be in demand in fundamental electrochemical investigations, whether they are directed towards bioanalysis, fuel cell technology, or materials research. It therefore appears certain that the UHV-EC approach will remain invaluable in the future.

REFERENCES

1. T. E. Furtak, K. L. Kliewer and D. W. Lynch, eds., "Non-Traditional Approaches to the Study of the Solid-Electrolyte Interface," North-Holland, Amsterdam (1980).
2. W. N. Hansen, D. M. Kolb and D. W. Lynch, eds., "Electronic and Molecular Structure of Electrode-Electrolyte Interfaces," Elsevier, Amsterdam (1983).
3. J. D. E. McIntyre and M. J. Weaver, eds., "The Chemistry and Physics of Electrocatalysis," The Electrochemical Society, Pennington (1984).
4. L. R. Faulkner, "*In Situ* Characterization of Electrochemical Processes," National Academy Press, Washington, D. C. (1987).
5. M. P. Soriaga, ed., "Electrochemical Surface Science," American Chemical Society, Washington, D. C. (1988).
6. J. Lipkowski and P. N. Ross, eds., "Adsorption of Molecules at Metal Electrodes," VCH Publishers, New York (1992).
7. J. Lipkowski and P. N. Ross, eds., "Structure of Electrified Interfaces," VCH Publishers, New York (1993).
8. G. A. Somorjai, "Chemistry in Two Dimensions: Surfaces," Cornell University, Ithaca (1981).
9. T. H. Rhodin and G. Ertl, eds., "The Nature of the Surface Chemical Bond," North-Holland Publishing, New York (1979).
10. G. Ertl and J. Kuppers, "Low Energy Electrons and Surface Chemistry," VCH Publishers, New York (1985).
11. D. P. Woodruff and T. A. Delchar, "Modern Techniques of Surface Science," Cambridge University Press, New York (1986).
12. A. Zangwill, "Physics at Surfaces," Cambridge University Press, New York (1988).
13. M. A. Van Hove, S. W. Wang, D. F. Ogletree and G. A. Somorjai, "*Adv. Quantum Chem.*, **20**, 1 (1989).
14. E. L. Muetterties, *Bull. Chim. Belg.*, **84**, 959 (1975).
15. E. L. Muetterties, *Bull. Chim. Belg.*, **85**, 451 (1976).
16. E. Shustorovich, R. C. Baetzold and E. L. Muetterties, *J. Phys. Chem.*, **87**, 1100 (1983).
17. R. Hoffman, "Solids and Surfaces: A Chemist's View of Bonding in Extended Structures," VCH Publishers, New York (1988).
18. M. R. Albert and J. T. Yates, Jr., "A Surface Scientist's Guide to Organometallic Chemistry," American Chemical Society, Washington, D. C. (1987).
19. A. B. Anderson, *J. Electroanal. Chem.*, **280**, 37 (1990).
20. A. B. Anderson. R. Kotz and E. Yeager, *Chem. Phys. Lett.*, **82**, 130 (1981).
21. S. P. Mehandru and A. B. Anderson, *J. Phys. Chem.*, **93**, 2044 (1989).
22. A. T. Hubbard, *Accts. Chem. Res.* **13**, 177 (1980).
23. A. T. Hubbard, *Chem. Rev.* **88**, 633 (1988).
24. P. N. Ross, in "Chemistry and Physics of Solid Surfaces," R. Vanselow and R. Howe, eds., Springer-Verlag, New York (1982).
25. E. Yeager, A. Homa, B. D. Cahan and D. Scherson, *J. Vac. Sci. Technol.*, **20**, 628 (1982).
26. D. M. Kolb, *Z. Phys. Chem. Neue Folge.*, **154**, 179 (1987).
27. D. M. Kolb, *Ber. Bunsenges. Phys. Chem.*, **92**, 1175 (1988).
28. M. P. Soriaga, *Prog. Surf. Sci.*, **39**, 325 (1992).
29. R. Adzic, in "Modern Aspects of Electrochemistry. XXI," R. E. White, J. O'M.

Bockris and B. E. Conway, eds., Plenum, New York (1990).
30. G. G. Will, *J. Electrochem. Soc.*, **112** 451 (1965).
31. A. T. Hubbard, R. P. Ishikawa and J. Katekaru, *J. Electroanal. Chem.*, **86**, 271 (1978).
32. J. Clavilier, *J. Electroanal. Chem.*, **107**, 205 (1980).
33. T. Solomun, B. C. Schardt, S. D. Rosasco, A. Wieckowski, J. L. Stickney and A. T. Hubbard, *J. Electroanal. Chem.*, **176**, 309 (1984).
34. R. R. Adzic, A. V. Tripkovic and V. B. Vesovic, *J. Electroanal. Chem.*, **204**, 329 (1986).
35. A. Rodes, J. M. Orts, J. M. Feliu, A. Aldaz and J. Clavilier, *J. Electroanal. Chem.*, **281**, 199 (1990).
36. E. A. Wood, "Crystal Orientation Manual," Columbia University Press, New York (1963).
37. B. Kaischew and B. Mutaftschiew, *Z. Phys. Chem.*, **204**, 334 (1955).
38. P. O. Nilsson and D. E. Eastman, *Phys. Scr.*, **8**, 113 (1973).
39. M. S. Zei, Y. Nakai, G. Lehmpfuhl and D. M. Kolb, *J. Electroanal. Chem.*, **150**, 201 (1983).
40. C. E. D. Chidsey, D. N. Loiacono, T. Sleator and S. Nakahara, *Surf. Sci.*, **200**, 45 (1988).
41. D. M. Kolb, G. Lempfuhl and M. S. Zei, *J. Electroanal. Chem.*, **179**, 289 (1984).
42. J. F. Rodriguez, M. E. Bothwell, G. J. Cali and M. P. Soriaga, *J. Am. Chem. Soc.*, **112** 7392 (1990).
43. G. J. Cali, G. M. Berry, M. E. Bothwell and M. P. Soriaga, *J. Electroanal. Chem.*, **297**, 523 (1991).
44. M. E. Bothwell, G. J. Cali, G. M. Berry and M. P. Soriaga, *Surf. Sci.*, **249**, L322 (1991).
45. A. Bewick and B. Thomas, *J. Electroanal. Chem.*, **65**, 911 (1975).
46. J. L. Stickney, I. Villegas and C. B. Ehlers. *J. Am. Chem. Soc.*, **111** 6473 (1989).
47. J. Clavilier, D. Armand, S. G. Sun and M. Petit, *J. Electroanal. Chem.*, **205**, 267 (1986).
48. D. Aberdam, R. Durand, R. Faure and F. El-Omar, *Surf. Sci.*, **171** 303 (1986).
49. J. Clavilier, in "Electrochemical Surface Science," M. P. Soriaga, ed., American Chemical Society, Washington, DC (1988).
50. D. J. Trevor, C. E. D. Chidsey and D. N. Loiacono, *Phys. Rev. Lett.*, **62**, 929 (1989).
51. E. Holland-Moritz, J. Gordon II, K. Kanazawa and R. Sonnenfeld, *Langmuir*, **7**, 1981 (1991).
52. P. N. Ross and F. T. Wagner, in "Advances in Electrochemistry and Electrochemical Engineering. XIII," H. Gerischer and C. W. Tobias, eds., Wiley-Interscience, New York (1984).
53. M. Hourani and A. Wieckowski, *J. Electroanal. Chem.*, **227**, 259 (1987).
54. M. Wasberg, L. Palaikis, S. Wallen, M. Kamrath and A. Wieckowski, *J. Electroanal. Chem.*, **256**, 51 (1988).
55. A. Wieckowski, in "Electrochemical Surface Science," M. P. Soriaga, ed., American Chemical Society, Washington, D. C. (1988).
56. H. H. Farrell and G. A. Somorjai, *Adv. Chem. Phys.*, **20**, 215 (1971).
57. M. A. van Hove and S. Y. Tong, "Surface Crystallography by LEED," Springer-Verlag, New York (1979).
58. C. Kittel, "Introduction to Solid-State Physics," Wiley, New York (1971).

59. A. Wieckowski, B. C. Schardt, S. D. Rosasco, J. L. Stickney and A. T. Hubbard, *Surf. Sci.*, **146**, 115 (1984).
60. A. W. Adamson, "Physical Chemistry of Surfaces," Wiley, New York (1990).
61. J. F. Rodriguez, T. Mebrahtu and M. P. Soriaga, *J. Electroanal. Chem.*, **264**, 291 (1989).
62. H. D. Hagstrum and G. E. Becker, *J. Vac. Sci. Technol.*, **14**, 369 (1977).
63. J. H. Neave, B. A. Joyce, P. J. Dobson and N. Norton, *Appl. Phys.*, **A31**, 1 (1983).
64. H. H. Madden, *Surf. Sci.*, **126**, 80 (1982).
65. D. R. Jennison, *J. Vac. Sci. Technol.*, **20**, 548 (1982).
66. R. R. Rye and J. E. Houston, *Accts. Chem. Res.*, **17**, 41 (1984).
67. K. W. Nebesny and N. R. Armstrong, *Langmuir*, **1**, 469 (1985).
68. K. W. Nebesny and N. R. Armstrong, *J. Electron Spectros.*, **37**, 355 (1986) 355.
69. M. C. Burrell and N. R. Armstrong, *Appl. Surf. Sci.*, **17**, 53 (1983).
70. R. E. Weber and W. T. Peria, *J. Appl. Phys.*, **38**, 4355 (1967).
71. J. M. Morabito, *Surf. Sci.*, **49**, 318 (1975).
72. W. A. Coghlan and R. E. Clausing, *At. Data*, **5**, 317 (1973).
73. J. Houston, *Surf. Sci.*, **38**, 283 (1973).
74. J. A. Schoeffel and A. T. Hubbard, *Anal. Chem.*, **49**, 2330 (1977).
75. B. C. Schardt, J. L. Stickney, D. A. Stern, D. G. Frank, J. Y. Katekaru, S. D. Rosasco, G. N. Salaita, M. P. Soriaga and A. T. Hubbard, *Inorg. Chem.*, **24**, 1419 (1985).
76. G. N. Salaita and A. T. Hubbard, in "Molecular Design of Electrode Surfaces," R. W. Murray, ed., Wiley, New York (1989).
77. C. J. Powell, *J. Vac. Sci. Technol.*, **A4**, 1532 (1986)
78. R. Payling, *J. Electron. Spect. Rel. Phenom.*, **37**, 225 (1985).
79. D. W. Suggs, I. Villegas, B. W. Gregory and J. L. Stickney. *Mater. Res. Soc. Symp. Proc.*, **222**, 283 (1991).
80. M. Gryzinski, *Phys. Rev.*, **A138**, 305 (1965).
81. T. A. Carlson, "Photoelectron and Auger Spectroscopy," Plenum, New York (1975).
82. C. S. Fadley, in "Electron Spectroscopy II," C. R. Bundle and A. D. Baker, eds., Academic, New York (1978).
83. K. Siegbahn, "ESCA, Atomic, Molecular and Solid State Structure Studies by Means of Electron Spectroscopy," Almqvist-Wiksell Boktryckeri, Sweden (1967).
84. M. P. Seah, in "Practical Surface Analysis by Auger and X-ray Photoelectron Spectroscopy," D. Briggs and M. P. Seah, eds., Wiley, New York (1983).
85. M. E. Hanson and E. Yeager, in "Electrochemical Surface Science," M. P. Soriaga, ed., American Chemical Society, Washington, D. C. (1988).
85. M. P. Soriaga, *Chem. Rev.*, **90**, 771 (1990).
86. H. Ibach and D. A. Mills, "Electron Energy Loss Spectroscopy," Academic, New York (1982).
87. N. R. Avery, in "Vibrational Spectroscopy of Molecules on Surfaces," J. T. Yates, Jr., and T. E. Madey, eds., Plenum, New York (1987).
88. F. M. Hoffman, *Surf. Sci. Reports*, **3**, 2 (1983).
89. B. E. Hayden, in "Vibrational Spectroscopy of Molecules on Surfaces," J. T. Yates, Jr., and T. E. Madey, eds., Plenum, New York (1987).
90. H. A. Pearce and N. Sheppard, *Surf. Sci.*, **59**, 205 (1976).
91. R. G. Greenler, in "Vibrations at Surfaces," R. Caudano, J. M. Giles and A. A.

Lucas, eds., Plenum, New York, (1982).
92. A. Bewick and B. S. Pons, in "Advances in Infrared and Raman Spectroscopy," R. J. H. Hester and R. E. Clark, eds., Wiley-Hayden, London (1985).
93. A. Bewick, J. M. Mellor and S. Pons, *Electrochim. Acta.*, **25**, 931 (1980).
94. S. Pons, *J. Electroanal. Chem.*, **150**, 495 (1983).
95. A. E. Dowrey and C. Marcott, *Appl. Spectr.*, **36**, 414 (1982).
96. W. G. Golden and D. D. Saperstein, *J. Electron Spectros.*, **30**, 43 (1983).
97. B. J. Barner, M. J. Green, E. I. Saez and R. M. Corn, *Anal. Chem.*, **63**, 55 (1991).
98. S. Pons and A. Bewick, *Langmuir*, **1**, 141 (1985).
99. N. Sheppard and T. T. Nguyen, in "Advances in Infrared and Raman Spectroscopy," R. E. Hester and R. J. H. Clark, eds., Wiley-Hayden, London (1978).
100. S. C. Chang and M. J. Weaver, *J. Phys. Chem.*, **95**, 3391 (1991).
101. W. Ho, R. R. Willis and E. W. Plummer, *Phys. Rev. Lett.*, **40**, 1463 (1978).
102. J. K. Foley and S. Pons, *Anal. Chem.*, **57**, 945A (1985).
103. H. Froitzheim, in "Topics in Current Physics. IV," H. Ibach, ed., Springer-Verlag, New York (1977).
104. C. Herring and M. H. Nichols, Rev. Mod. Phys., **21**, 185 (1949).
105. H. Reiss, *J. Phys. Chem.*, **89**, 3783 (1985).
106. W. N. Hansen, *J. Electroanal. Chem.*, **150**, 133 (1983).
107. W. N. Hansen and G. J. Hansen, in "Electrochemical Surface Science," M, P, Soriaga, ed., American Chemical Society, Washington, D. C. (1988).
108. P. A. Redhead, *Vacuum*, **12**, 203 (1962).
109. H. A. Strobel and W. R. Heineman, "Chemical Instrumentation," Wiley, New York (1989).
110. J. S. Hammond and N. Winograd, *J. Electroanal. Chem.*, **78**, 55 (1977).
111. A. T. Hubbard. *J. Vac. Sci. Technol.*, **17**, 49 (1980).
112. J. L. Stickney, C. B. Ehlers and B. W. Gregory, in "Electrochemical Surface Science," M. P. Soriaga, ed., American Chemical Society, Washington, D. C. (1988).
113. T. Mebrahtu, J. F. Rodriguez, M. E. Bothwell, I. F. Cheng, D. R. Lawson, J. R. McBride, C. R. Martin and M. P. Soriaga, *J. Electroanal. Chem.*, **267**, 351 (1989).
114. T. Solomun, W. Richtering and H. Gerischer, *Ber. Bunsenges. Phys. Chem.*, **91**, 412 (1987).
115. K. R. Zavadil and N. R. Armstrong, *J. Electrochem. Soc.*, **137**, 2371 (1990).
116. L.-W. H. Leung, T. W. Gregg and D. W. Goodman, *Rev. Sci. Instrum.*, **62**, 1857 (1991).
117. B. E. Conway, H. Angerstein-Kozlowska, W. B. A. Sharp and E. E. Criddle, *Anal. Chem.*, **45**, 1331 (1973).
118. W. Hansen and D. M. Kolb, *J. Electroanal. Chem.*, **100**, 493 (1979).
119. D. Rath and D. M. Kolb, *Surf. Sci.*, **109**, 641 (1981).
120. G. J. Hansen and W. N. Hansen, *J. Electroanal. Chem.*, **150**, 193 (1983).
121. W. N. Hansen. *Surf. Sci.*, **101** 109 (1980).
122. J. D. E. McIntyre, *Adv. Electrochem. Electrochem. Engr.*, **9**, 61 (1973).
123. W. Hansen, D. M. Kolb, D. Rath and R. Wille, *J. Electroanal. Chem.*, **110** 369 (1980).
124. O. Hofman, K. Doblhofer and H. Gerischer, *J. Electroanal. Chem.*, **161** 337 (1984).

125. G. J. Hansen and W. N. Hansen, *Ber. Bunsenges. Phys. Chem.*, **91**, 317 (1987).
126. J. E. Pemberton, R. L. Sobocinksi and M. A. Bryant, *J. Am. Chem. Soc.*, **112** 6177 (1990).
127. J. E. Pemberton and R. L. Sobocinksi, *J. Electroanal. Chem.*, **318**, 157 (1991).
128. E. R. Koetz, H. Neff and R. H. Muller, *J. Electroanal. Chem.*, **215**, 331 (1986).
129. Z. Samec, B. W. Johnson and K. Doblhofer, *Surf. Sci.*, **264**, 400 (1992).
130. S. D. Rosasco, J. L. Stickney, G. N. Salaita, D. G. Frank, J. Y. Katekaru, B. C. Schardt, M. P. Soriaga, D. A. Stern and A. T. Hubbard, *J. Electroanal. Chem.*, **188**, 95 (1985).
131. D. G. Frank, J. Y. Katekaru, S. D. Rosasco, G. N. Salaita, B. C. Schardt, M. P. Soriaga, J. L. Stickney and A. T. Hubbard, *Langmuir*, **1**, 587 (1985).
132. D. A. Stern, L. Laguren-Davidson, F. Lu, C. H. Lin, D. G. Frank, G. N. Salaita, N. Walton, J. Y. Gui, D. C. Zapien and A. T. Hubbard, *J. Am. Chem. Soc.*, **111**, 877 (1989).
133. T. E. Madey and F. P. Netzer, *Surf. Sci.*, **117**, 549 (1980).
134. J. K. Sass, K. Kretzschmar and S. Holloway, *Vacuum*, **31**, 483 (1981).
135. J. K. Sass. *Vacuum*, **33**, 741 (1983).
136. J. K. Sass and K. Bange, in "Electrochemical Surface Science," M. P. Soriaga, ed., American Chemical Society, Washington, D. C. (1988).
137. J. K. Sass, K. Bange, R. Dohl, E. Plitz and R. Unwin, *Ber. Bunsenges, Phys. Chem.*, **88**, 354 (1984).
138. K. Bange, B. Straehler, J. K. Sass and R. Parsons, *J. Electroanal. Chem.*, **229**, 87 (1987)
139. F. T. Wagner, S. J. Schmieg and T. E. Moylan, *Surf. Sci.*, **195**, 403 (1988).
140. F. T. Wagner and T. E. Moylan, in "Electrochemical Surface Science," M. P. Soriaga, ed., American Chemical Society, Washington, D. C. (1988).
141. D. A. Stern, H. Baltruschat, M. Martinez, J. L. Stickney, D. Song, S. K. Lewis, D. G. Frank and A. T. Hubbard, *J. Electroanal. Chem.*, **217**, 101 (1987).
142. G. N. Salaita, D. A. Stern, F. Lu, H. Baltruschat, B. C. Schardt, J. L. Stickney, M. P. Soriaga, D. G. Frank and A. T. Hubbard, *Langmuir*, **2**, 828 (1986).
143. F. Lu, G. N. Salaita, H. Baltruschat and A. T. Hubbard, *J. Electroanal. Chem.*, **222**, 305 (1987).
144. N. Batina, J. W. McCargar, L. Laguren-Davidson, C.-H. Lin and A. T. Hubbard, *Langmuir*, **5**, 123 (1989).
145. J. L. Stickney, S. D. Rosasco, G. N. Salaita and A. T. Hubbard, *Langmuir*, **1**, 66 (1985).
146. G. A. Garwood and A. T. Hubbard. *Surf. Sci.*, **112**, 281 (1982).
147. G. A. Garwood and A. T. Hubbard. *Surf. Sci.*, **121**, 396 (1982).
148. T. Solomun, A. Wieckowski, S. D. Rosasco and A. T. Hubbard, *Surf. Sci*, **147**, 241 (1984).
149. C. B. Ehlers and J. L. Stickney, *Surf. Sci.*, **239**, 85 (1990).
150. G. N. Salaita, F. Lu, L. Laguren-Davidson and A. T. Hubbard, *J. Electroanal. Chem.*, **229**, 1 (1987).
151. B. G. Bravo, S. L. Michelhaugh, M. P. Soriaga, I. Villegas, D. W. Suggs and J. L. Stickney, *J. Phys. Chem.*, **95**, 5245 (1991).
152. T. Mebrahtu, M. E. Bothwell, J. E. Harris, G. J. Cali and M. P. Soriaga, *J. Electroanal. Chem.*, **300**, 487 (1991).
153. T. E. Felter and A. T. Hubbard, *J. Electroanal. Chem.*, **100**, 473 (1979).
154. G. A. Garwood, Jr. and A. T. Hubbard, *Surf. Sci.*, **92**, 617 (1980).

155. P. N. Ross, in "Electrochemical Surface Science," M. P. Soriaga, ed., American Chemical Society, Washington, D. C. (1988).
156. J. Clavilier, A. Rodes, K. El Achi and M. A. Zamakhchari, *J. Chim. Phys.*, **88**, 1291 (1991).
157. F. T. Wagner and P. N. Ross, *Surf. Sci.*, **160**, 305 (1985).
158. J. Horkans, B. D. Cahan and E. Yeager, *Surf. Sci.*, **37**, 559 (1973).
159. F. T. Wagner and P. N. Ross, *J. Electroanal. Chem.*, **150**, 141 (1985).
160. J. B. Lumsden. G. A. Garwood and A. T. Hubbard, *Surf. Sci.* **121**, 1524 (1982).
161. D. A. Harrington, A. Wieckowski, S. D. Rosasco, B. C. Schardt, G. N. Salaita, J. B. Lumsden and A. T. Hubbard, *Corrosion Sci.*, **25**, 849 (1985).
162. D. A. Harrington, A. Wieckowski, S. D. Rosasco, B. C. Schardt, G. N. Salaita and A. T. Hubbard, *Langmuir*, **1**, 232 (1985).
163. J. P. Biberian and G. A. Somorjai. *J. Vac. Sci. Technol.*, **16**, 2073 (1979).
164. J. S. Hammond and N. Winograd, *J. Electroanal. Chem.*, **80**, 123 (1977).
165. J. S. Hammond and N. Winograd, *J. Electrochem. Soc.*, **124**, 826 (1977).
166. A. T. Hubbard, J. L. Stickney, S. D. Rosasco, M. P. Soriaga and D. Song, *J. Electroanal. Chem.*, **150**, 165 (1983).
167. J. L. Stickney, S. D. Rosasco, M. P. Soriaga, D. Song and A. T. Hubbard, *Surf. Sci.*, **130**, 326 (1983).
168. J. L. Stickney, S. D. Rosasco, B. C. Schardt and A.T. Hubbard, *J. Phys. Chem.*, **88**, 251 (1984).
169. J. L. Stickney, S. D. Rosasco and A.T. Hubbard, *J. Electrochem. Soc.*, **131**, 260 (1984).
170. J. L. Stickney, D. A. Stern, B. C. Schardt, D. C. Zapien, A. Wieckowski and A.T. Hubbard, *J. Electroanal. Chem.*, **213**, 293 (1986).
171. J. L. Stickney, B. C. Schardt, D. A. Stern, A. Wieckowski and A.T. Hubbard, *J. Electrochem. Soc.*, **133**, 648 (1986).
172. B. C. Schardt, J. L. Stickney, D. A. Stern, A. Wieckowski, D. C. Zapien and A. T. Hubbard, *Langmuir*, **3**, 239 (1987).
173. B. C. Schardt, J. L. Stickney, D. A. Stern, A. Wieckowski, D. C. Zapien and A. T. Hubbard, *Surf. Sci.*, **175**, 520 (1986).
174. P. C. Andricacos and P. N. Ross, *J. Electroanal. Chem.*, **167**, 301 (1984).
175. D. Aberdam, R. Durand, R. Faure and F. El-Omar, *Surf. Sci.*, **162**, 782 (1985).
176. L.-W. H. Leung, T. W. Gregg and D. W. Goodman. *Langmuir*, **7**, 3205 (1991).
177. L. Laguren-Davidson, F. Lu, G. N. Salaita and A. T. Hubbard, *Langmuir*, **4**, 224 (1988).
178. B. W. Gregory and J. L. Stickney, *J. Electroanal. Chem.*, **300**, 543 (1991).
179. D. W. Suggs and J. L. Stickney, *J. Phys. Chem.*, **95**, 10056 (1991).
180. P. N. Ross, *J. Chim. Phys.*, **88**, 1353 (1991).
181. P. Faguy, N. Markovic, R. Adzic, C. Fieiro and E. Yeager, *J. Electroanal. Chem.*, **289**, 245 (1990).
182. M. P. Soriaga, in "Structure of Electrified Interfaces," J. Lipkowski and P. N. Ross, eds., VCH Publishers, New York (1993).
183. B. B. Damaskin and A. N. Frumkin, *Electrochim. Acta*, **19**, 173 (1974).
184. R. Parsons, *J. Electroanal. Chem.*, **59**, 229 (1975).
185. P. A. Thiel and T. E. Madey, *Surf. Sci. Rep.*, **7**, 211 (1987).
186. F. T. Wagner and T. E. Moylan, *Surf. Sci.*, **182**, 125 (1987).
187. E. M. Stuve, R. Dohl-Oelze, C. C. Brown and S. Stark. *Surf. Sci.* **210**, 339 (1989).
188. C. K. Mann and K. K. Barnes, "Electrochemical Reactions in Nonaqueous Solvents," Marcel Dekker, New York (1970).

189. H. Ohtani, C. T. Kao, M. A. Van Hove and G. A. Somorjai, *Prog. Surf. Sci.*, **23**, 155 (1987).
190. G. A. Garwood, Jr. and A. T. Hubbard, *Surf. Sci.*, **118** 233 (1982).
191. J. Y. Gui, F. Lu, D. A. Stern and A. T. Hubbard, *J. Electroanal. Chem.*, **292**, 245 (1990).
192. B. B. Damaskin, O. A. Petrii and V. V. Batrakov, "Adsorption of Organic Compounds on Electrodes," Plenum, New York (1971).
193. G. Horanyi, *J. Electroanal. Chem.*, **51**, 163 (1974).
194. R. D. Snell and A. G. Keenan, *Chem. Soc. Rev.*, **8**, 259 (1979).
195. A. Wieckowski, *Electrochim. Acta*, **26**, 1121 (1981).
196. J. L. Stickney, M. P. Soriaga, A.T. Hubbard and S. E. Anderson, *J. Electroanal. Chem.*, **125**, 73 (1981).
197. S. L. Michelhaugh, C. Bhardwaj, G. J. Cali, B. G. Bravo, M. E. Bothwell, G. M. Berry and M. P. Soriaga, *Corrosion*, **47**, 322 (1991).
198. D. Zurawski, M. Wasberg and A. Wieckowski, *J. Phys. Chem.*, **94**, 2076 (1990).
199. G. M. Berry, M. E. Bothwell, S. L. Michelhaugh, J. R. McBride and M. P. Soriaga, *J. Chim. Phys.*, **88**, 1591 (1991).
200. A. T. Hubbard, D. A. Stern, G. N. Salaita, D. G. Frank, F. Lu, L. Laguren-Davidson, N. Batina and D. C. Zapien, in "Electrochemical Surface Science," M. P. Soriaga, ed., American Chemical Society, Washington, D. C. (1988).
201. A. T. Hubbard and J. Y. Gui, *J. Chim. Phys.*, **88**, 1547 (1991).
202. D. Zurawski and A. Wieckowski, *Langmuir*, **8**, 2317 (1992).
203. K. Wang, G. S. Chottiner and D. A. Scherson. *J. Phys. Chem.* **96**, 6742 (1992).
204. A. Wieckowski, S. D. Rosasco, G. N. Salaita, A. T. Hubbard, B. E. Bent, F. Zaera, D. Godbey and G. A. Somorjai, *J. Am. Chem. Soc.*, **107**, 5910 (1985).
205. A. T. Hubbard, M. A. Young and J. A. Schoeffel, *J. Electroanal. Chem.*, **114** 273 (1980).
206. M. Hourani and A. Wieckowski, *Langmuir*, **6**, 379 (1990).
207. N. Batina, S. A. Chaffins, J. Y. Gui, F. Lu, J. W. McCargar, J. W. Rovang, D. A. Stern and A. T. Hubbard, *J. Electroanal. Chem.*, **284**, 81 (1990).
208. N. Batina, J. W. McCargar, C. H. Lin, G. N. Salaita, B. E. Kahn and A. T. Hubbard, *Electroanal.*, **1**, 213 (1989).
209. J. Y. Gui, D. A. Stern, D. C. Zapien, G. N. Salaita, F. Lu, C. H. Lin, B. E. Kahn and A. T. Hubbard, *J. Electroanal. Chem.*, **252**, 169 (1988).
210. B. E. Kahn, S. A. Chaffins, J. Y. Gui, F. Lu, D. A. Stern and A. T. Hubbard, *Chem. Phys.*, **141** 21 (1990).
211. G. N. Salaita, C. Lin, P. Gao and A. T. Hubbard, *Arabian J. Sci. Engr.*, **15**, 319 (1990).
212. J. Y. Gui, L. Laguren-Davidson, C. H. Lin, F. Lu, G. N. Salaita, D. A. Stern, B. E. Kahn and A. T. Hubbard, *Langmuir*, **5**, 819 (1989).
213. N. Batina, D. C. Zapien, F. Lu, C. H. Lin, McCargar, B. E. Kahn, J. Y. Gui, D. G. Frank, G. N. Salaita, D. A. Stern and A. T. Hubbard, *Electrochim. Acta*, **34**, 1031 (1989).
214. S. A. Chaffins, J. Y. Gui, C. H. Lin, F. Lu, G. N. Salaita, D. A. Stern, B. E. Kahn and A. T. Hubbard, *J. Electroanal. Chem.*, **284**, 67 (1990).
215. M. P. Soriaga and A. T. Hubbard. *J. Am. Chem. Soc.*, **104**, 2735 (1982).
216. M. P. Soriaga and A. T. Hubbard. *J. Am. Chem. Soc.*, **104**, 2742 (1982).
217. M. P. Soriaga and A. T. Hubbard, *J. Am. Chem. Soc.*, **104**, 3937 (1982).
218. M. P. Soriaga, P. H. Wilson, A. T. Hubbard and C. S. Benton, *J. Electroanal. Chem.*, **142**, 317 (1982).

219. M. P. Soriaga, J. H. White and A. T. Hubbard, *J. Phys. Chem.*, **87**, 3048 (1983).
220. M. P. Soriaga, E. Binamira-Soriaga, A. T. Hubbard, J. B. Benziger and K. W. P. Pang, *Inorg. Chem.*, **24**, 65 (1985).
221. M. P. Soriaga, J. H. White, V. K. F. Chia, D. Song, P. O. Arrhenius and A. T. Hubbard, *Inorg. Chem.*, **24**, 73 (1985).
222. M. P. Soriaga, J. L. Stickney and A. T. Hubbard. *J. Mol. Catal.*, **21**, 211 (1983).
223. M. P. Soriaga, J. L. Stickney and A. T. Hubbard, *J. Electroanal. Chem.*, **144**, 207 (1983).
224. M. P. Soriaga and A. T. Hubbard, *J. Phys. Chem.*, **88**, 1758 (1984).
225. N. Batina, B. E. Kahn, J. Y. Gui, F. Lu, J. W. McCargar, H. B. Mark, C. H. Lin, B. N. Salaita, H. Zimmer, D. A. Stern and A. T. Hubbard, *Langmuir*, **5**, 588 (1989).
226. D. A. Stern, L. Laguren-Davidson, F. Lu, C. H. Lin, D. G. Frank, G. N. Salaita, N. Walton, J. Y. Gui, D. C. Zapien and A. T. Hubbard, *J. Am. Chem. Soc.*, **111** 877 (1989).
227. S. A. Chaffins, J. Y. Gui, B. E. Kahn, C. H. Lin, F. Lu, G. N. Salaita, D. A. Stern, D. C. Zapien, A. T. Hubbard and C. M. Elliott, *Langmuir*, **6**, 951 (1990).
228. S. A. Chaffins, J. Y. Gui, C. H. Lin, F. Lu, G. N. Salaita, D. A. Stern and A. T. Hubbard, *Langmuir*, **6**, 1273 (1990).
229. A. T. Hubbard, D. G. Frank, D. A. Stern, M. J. Tarlov, N. Batina, N. Walton, E. Wellner and J. W. McCargar, in "Redox Chemistry and Interfacial Behavior of Biological Molecules," G. Dryhurst and R. Niki, eds., Plenum, New York (1988).
230. D. A. Stern, N. Walton, J. W. McCargar, G. N. Salaita, L. Laguren-Davidson, F. Lu, C. H. Lin, J. Y. Gui, N. Batina, D. G. Frank and A. T. Hubbard, *Langmuir*, **4**, 711 (1988).